

Critical pairing fluctuations in the normal state of a superconductor: pseudogap and quasi-particle damping

Philipp Lange, Oleksandr Tsyplyatyev, and Peter Kopietz
*Institut für Theoretische Physik, Universität Frankfurt,
 Max-von-Laue Strasse 1, 60438 Frankfurt, Germany*
 (Dated: April 18, 2017)

We study the effect of critical pairing fluctuations on the electronic properties in the normal state of a clean superconductor in three dimensions. Using a functional renormalization group approach to take the non-Gaussian nature of critical fluctuations into account, we show microscopically that in the BCS regime, where the inverse coherence length is much smaller than the Fermi wavevector, critical pairing fluctuations give rise to a non-analytic contribution to the quasi-particle damping of order $T_c \sqrt{Gi} \ln(80/Gi)$, where the Ginzburg-Levanyuk number Gi is a dimensionless measure for the width of the critical region. As a consequence, there is a temperature window above T_c where the quasiparticle damping due to critical pairing fluctuations can be larger than the usual T^2 -Fermi liquid damping due to non-critical scattering processes. On the other hand, in the strong coupling regime where Gi is of order unity, we find that the quasiparticle damping due to critical pairing fluctuations is proportional to the temperature. Moreover, we show that in the vicinity of the critical temperature T_c the electronic density of states exhibits a fluctuation-induced pseudogap. We also use functional renormalization group methods to derive and classify various types of processes induced by the pairing interaction in Fermi systems close to the superconducting instability.

I. INTRODUCTION

The BCS mean-field theory has been tremendously successful to explain the physical properties of superconductors, but the true critical behavior of the classical phase transition between a normal metal and a superconductor is not mean-field like but belongs to the universality class of the classical XY-model. Fortunately, in conventional superconductors the critical region where fluctuation effects are important is extremely small, so that for all practical purposes the mean-field approximation is sufficient.¹ The smallness of the critical region in weakly coupled BCS superconductors is due to the fact that in these systems the zero temperature coherence length ξ_0 , which measures the typical size of the Cooper pairs, is many orders of magnitude larger than the lattice spacing. A dimensionless measure of the temperature range δT around the critical temperature T_c where fluctuations are important is given by the Ginzburg-Levanyuk number^{2,3} Gi , which for a clean three-dimensional superconductor can be written as¹

$$Gi = \frac{\delta T}{T_c} \approx 0.8 \left(\frac{\pi T_c}{E_F} \right)^4, \quad (1.1)$$

where E_F is the Fermi energy. In the weak coupling BCS regime the value of Gi is typically in the range between 10^{-14} and 10^{-12} , so that the critical region cannot be resolved experimentally. On the other hand, in strongly correlated superconductors the inverse coherence length $1/\xi_0$ can have the same order of magnitude as the Fermi momentum k_F . In this case Gi is of the order of unity and the critical regime is experimentally accessible. Another class of experimentally tunable systems where fluctuations of the superfluid order parameter cannot be neglected are the ultracold fermions with attractive interaction in the vicinity of the unitary point where the two-

body scattering length diverges.⁴

Although fluctuation effects in superconductors and superfluids have been studied for many decades,¹ there are still some open questions. In particular, the renormalization of the electronic single-particle excitations in the normal state at or slightly above the critical temperature are not completely understood. In a seminal work by Aslamazov and Larkin,⁵ the transport time and its effect on conductivity were shown to be divergent at the transition temperature within the ladder approximation. The effect of superconducting fluctuations on the density of states and the tunneling resistance has been studied within a perturbative approach to first order in the strength of the superconducting interaction.⁶ This approximation is expected to break down sufficiently close to the critical temperature,¹ where the non-Gaussian nature of the pairing fluctuations and the renormalization of the electronic single-particle excitations must be taken into account. The single-particle spectral function was calculated numerically in Refs. [7] and [8] using the same ladder approximation, which corresponds to treating fluctuations of the superconducting order parameter only on the Gaussian level. To the best of our knowledge, a quantitative analysis of the electronic density of states and the quasi-particle damping beyond this approximation does not exist in the literature. In the superconducting phase, the modification of the electronic density of states due to Gaussian order parameter fluctuations has been studied by Lerch *et al.*,⁹ who found an unexpected logarithmic renormalization of the BCS result. In the present work we focus on the temperature regime above the critical temperature T_c where the system is in the normal state and hence the anomalous part of the electronic self-energy vanishes. This simplifies the calculations and enables us to include the effect of non-Gaussian critical order-parameter fluctuations on

the single-particle spectrum using renormalization group methods.

Diagrammatically, retaining Gaussian fluctuations of the superconducting order parameter is equivalent to calculating the effective two-body interaction between fermions in ladder approximation, which amounts to solving the Bethe-Salpeter equation for the effective interaction in the particle-particle channel.¹ Higher order interaction processes involving fluctuations with arbitrary momentum transfer give rise to non-Gaussian order parameter fluctuations. The next order effect of the pairing coupling on the critical temperature of a weakly interacting superconductor in the BCS regime has first been calculated by Gorkov and Melik-Barkhudarov (GM),¹⁰ who showed that even for arbitrarily weak bare interaction the fluctuations lead to a finite decrease of the critical temperature. In recent years the effects of induced interactions due to non-Gaussian pairing fluctuations have been studied for various other setups, such as systems involving more than two fermion flavors,¹¹ effective models describing the crossover from a BCS superconductor to a Bose-Einstein condensate (BCS-BEC crossover),^{12–14} and multi-band models describing the iron-based superconductors.¹⁵ Moreover, it has been shown¹⁶ that in the vicinity of a nematic quantum critical point the induced interactions mediated by soft fluctuations associated with the nematic order parameter can enhance the critical temperature for superconductivity.

In this work we use a functional renormalization group (FRG) approach^{17,18} to derive and classify the induced interactions responsible for the corrections to BCS theory. Our approach is based on the vertex expansion and partial bosonization in the particle-particle channel,^{17,19} and is therefore complementary to recent work by Tanizaki *et al.*,²⁰ who have used a purely fermionic formulation of the FRG to calculate the correction to the BCS result for T_c due to pairing fluctuations. Our main focus is the effect of critical pairing fluctuations on the spectrum of single-particle excitations in the normal state.

Let us give a brief overview of the rest of this work and summarize our main results. In Sec. II we derive an effective field theory describing normal fermions which are coupled to pairing fluctuations. We also show how the GM correction¹⁰ to the critical temperature T_c can be obtained within our approach, and that the GM result for T_c is modified if the chemical potential (and not the density of the electrons) is held constant. Our FRG approach for this model is developed in Sec. III, where we also explain the emergence of various types of induced interaction processes due to pairing fluctuations from the renormalization group point of view.

In Sec. IV we then discuss the effect of pairing fluctuations of the superconducting order parameter on the fermionic self-energy and the density of states within the ladder approximation. We show that in this approximation the density of states exhibits a finite pseudogap but the damping of quasiparticles with momenta

on the Fermi surface still diverges logarithmically as $\ln[T_c/(T - T_c)]$ for $T \rightarrow T_c$. While the emergence of a pseudogap due to fluctuations above T_c has been intensely investigated in the past,^{21–25} it is somewhat surprising that the logarithmic divergence of the quasiparticle damping in a clean three-dimensional superconductor has not been noticed in the previous literature on the subject.¹ This singularity can be cured by taking into account the finite lifetime of the quasiparticles in intermediate states, or by including non-Gaussian critical pairing fluctuations which generate a finite anomalous dimension η of the pairing fluctuations. In Sec. III we take both effects consistently into account using a specific implementation of the FRG. We find that the quasiparticle damping at $T = T_c$ due to critical order-parameter fluctuations has in the BCS regime the non-analytic form,

$$\gamma_{\text{crit}} \approx C \frac{T_c^3}{E_F^2} \ln\left(\frac{E_F}{T_c}\right) \approx T_c \sqrt{Gi} \ln\left(\frac{80}{Gi}\right), \quad (1.2)$$

where our estimate for the numerical prefactor is $C \approx 30$. Due to the rather large value of C , in a sizable regime of temperatures close to T_c the critical contribution (1.2) to the quasiparticle damping dominates the usual T^2 -Fermi liquid behavior due to non-critical interaction processes, as illustrated in Fig. 16 below. Moreover, we also show that in the strongly interacting superconductors, where the inverse coherence length can have the same order of magnitude as the Fermi momentum k_F , the quasiparticle damping due to critical order-parameter fluctuations is proportional to the temperature. Finally, in Sec. V we present our conclusions and discuss possible extensions of the methods developed in this work.

Further technical details are given in five appendices. In Appendix A we discuss in detail the approximations which are necessary to derive the GM result¹⁰ for the critical temperature from the interaction corrections to the particle-particle bubble. In Appendix B we write down exact FRG flow equations for the induced interactions in our model. The momentum-dependence of the non-interacting particle-particle bubble is derived in Appendix C, while in Appendix D we justify why in the vicinity of T_c it is sufficient to retain only the zeroth Matsubara frequency (associated with classical fluctuations) in the bosonic correlation function. Finally, in Appendix F we improve the FRG calculation of the quasiparticle damping of Sec. IV B by taking into account higher order vertex corrections.

II. INDUCED INTERACTIONS IN FERMIONIC SUPERFLUIDS

A. Effective field theory for superfluid fluctuations

We consider a system of electrons with quadratic energy dispersion $\epsilon_{\mathbf{k}} = \mathbf{k}^2/(2m)$ which are coupled by a short-range attractive two-body interaction with

strength $g_0 > 0$. The coupling g_0 represents some effective interaction in the spin-singlet particle-particle channel. Since we neglect long-range Coulomb interactions and do not consider the coupling to external electromagnetic fields, we do not distinguish between superfluidity and superconductivity. At finite temperature T and chemical potential μ the Euclidean action of the system is

$$S[\bar{c}, c] = \int_K \sum_{\sigma} (-i\omega + \epsilon_{\mathbf{k}} - \mu) \bar{c}_{K\sigma} c_{K\sigma} - g_0 \int_P \bar{C}_P C_P, \quad (2.1)$$

where $c_{K\sigma}$ and $\bar{c}_{K\sigma}$ are Grassmann fields labeled by momentum \mathbf{k} , Matsubara frequencies $i\omega$, and spin projection $\sigma = \uparrow, \downarrow$ (we introduce collective labels $K = (\mathbf{k}, i\omega)$ and use units where \hbar and the Boltzmann constant can be set equal to unity), and the collective fields C_P and \bar{C}_P are defined by

$$C_P = \int_K c_{-K\downarrow} c_{K+P\uparrow}, \quad (2.2a)$$

$$\bar{C}_P = \int_K \bar{c}_{K+P\uparrow} \bar{c}_{-K\downarrow}. \quad (2.2b)$$

Here $P = (\mathbf{p}, i\bar{\omega})$ represents the total (bosonic) Matsubara frequency $i\bar{\omega}$ and the total momentum \mathbf{p} of a pair of electrons with opposite spin, and the integration symbols are defined by $\int_K = T \sum_{\omega} \int d^D k / (2\pi)^D$ and $\int_P = T \sum_{\bar{\omega}} \int d^D p / (2\pi)^D$. Although we are eventually interested in $D = 3$ dimensions, we will keep D arbitrary before we explicitly start evaluating momentum integrals. We represent the bare interaction of our model defined in Eq. (2.1) by the graphical element shown in Fig. 1 (a). The physics in the vicinity of the superfluid transition is dominated by the effective interaction in the particle-particle channel. It is then natural to decouple the two-body interaction in Eq. (2.1) by means of a complex bosonic Hubbard-Stratonovich field ψ such that the composite particle-particle fields defined in Eqs. (2.2a) and (2.2b) appear in the decoupled action, which then assumes the form

$$S[\bar{c}, c, \bar{\psi}, \psi] = - \int_K \sum_{\sigma} G_0^{-1}(K) \bar{c}_{K\sigma} c_{K\sigma} + \int_P g_0^{-1} \bar{\psi}_P \psi_P + \int_P [\bar{C}_P \psi_P + C_P \bar{\psi}_P], \quad (2.3)$$

where we have introduced the bare fermion propagator

$$G_0(K) = \frac{1}{i\omega - \epsilon_{\mathbf{k}} + \mu}. \quad (2.4)$$

The interaction in the last term of Eq. (2.3) involves three-legged (Yukawa) vertices with one bosonic and two fermionic external legs, as shown in Fig. 1 (b). We shall refer to ψ as the order parameter field, because a finite expectation value of this field signals the existence of superfluidity in the system. In this work, we shall focus on the temperature regime above the superfluid critical

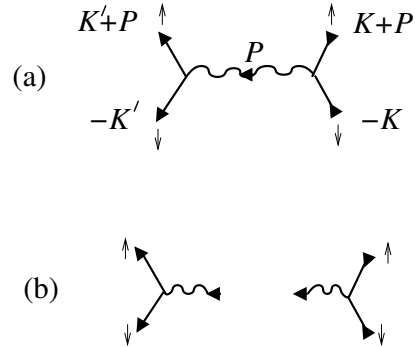


FIG. 1. (a) Graphical representation of the bare interaction in Eq. (2.1). The wavy arrow represents the bare coupling constant g_0 , where the arrow indicates the flow of the total energy-momentum P carried by the interaction. Incoming external arrows represent c_{σ} while outgoing arrows represent \bar{c}_{σ} . The spin projections $\sigma = \uparrow, \downarrow$ and the energy-momentum labels are written next to the legs. (b) Equivalent three-legged vertices after Hubbard-Stratonovich transformation in the particle-particle channel, see Eq. (2.3). Incoming wavy arrows represent the bosonic Hubbard-Stratonovich field ψ , while incoming wavy arrows represent the complex conjugate field $\bar{\psi}$.

temperature. In this case the exact fermionic propagator is given by

$$G(K) = \frac{1}{G_0(K)^{-1} - \Sigma(K)}, \quad (2.5)$$

where $\Sigma(K)$ is the exact fermionic self-energy in the normal state. Similarly, the exact propagator of our order parameter field is of the form

$$F(P) = \frac{1}{g_0^{-1} - \Phi(P)}, \quad (2.6)$$

where the function $\Phi(P)$ can be identified with the one-interaction-line irreducible bosonic self-energy. Graphical representations of the two Dyson equations (2.5) and (2.6) are shown in Fig. 2. Note that in lowest order perturbation theory $\Phi(P) \approx \Phi_0(P)$ can be identified with the particle-particle bubble with bare fermionic propagators,

$$\Phi_0(P) = \int_K G_0(K) G_0(P - K). \quad (2.7)$$

The transition temperature to the superfluid state can be determined from the condition that the order-parameter field for $P = 0$ becomes gapless at $T = T_c$, i.e.,

$$F^{-1}(P = 0) = g_0^{-1} - \Phi(P = 0) = 0, \quad (2.8)$$

which is equivalent with the statement that the corresponding uniform susceptibility diverges. To determine the critical temperature T_c for superfluidity, we should

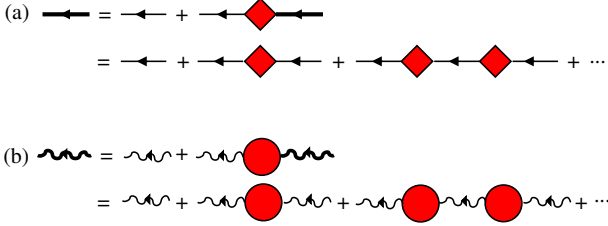


FIG. 2. Dyson equations for the fermionic and bosonic propagators. (a) represents the Dyson equation (2.5) for the fermionic propagator, denoted by a thick solid arrow. The thin solid arrows represent the bare fermionic propagator while the one-particle irreducible self-energy $\Sigma(K)$ is represented by a shaded box. (b) represents the corresponding bosonic Dyson equation (2.6). Here the thick wavy arrow represents the exact bosonic propagator, while the thin wavy arrow represents the bare interaction. The shaded circle represents the one-interaction-line irreducible bosonic self-energy $\Phi(P)$, which can be identified with the exact irreducible particle-particle bubble.

calculate the function $\Phi(0) = \Phi(\mathbf{p} = 0, i\bar{\omega} = 0)$ to a certain approximation and then tune the temperature T such that Eq. (2.8) is satisfied. The corrections to the non-interacting bubble given in Eq. (2.7) can be expressed in terms of the induced interactions, which take scattering processes in all channels into account. Although the Hubbard-Stratonovich transformed bare action (2.3) does not contain two-body and higher order interaction vertices, these vertices will appear in the effective low-energy theory when we integrate out high-energy degrees of freedom. In particular, two types of fermionic two-body interaction vertices will be generated, which we denote by $\Gamma^{\bar{c}_\uparrow \bar{c}_\downarrow c_\downarrow c_\uparrow}(K'_1, K'_2; K_2, K_1)$, and $\Gamma^{\bar{c}_\sigma \bar{c}_\sigma c_\sigma c_\sigma}(K'_1, K'_2; K_2, K_1)$, where $\sigma = \uparrow, \downarrow$ and the superscripts denote the field types associated with the external legs and the energy-momentum labels refer to the corresponding superscripts. Moreover, the two-body interactions between the superfluid order parameter are encoded in the bosonic interaction vertex $\Gamma^{\bar{\psi} \bar{\psi} \psi \psi}(P'_1, P'_2; P_2, P_1)$. Finally, symmetry allows also mixed four-point vertices $\Gamma^{\bar{c}_\sigma c_\sigma \bar{\psi} \psi}(K'; K; P'; P)$ with two fermionic and two bosonic external legs. Graphical representations of these different types of induced interaction vertices are shown in Fig. 3.

B. Skeleton equations

Before calculating the fermionic and bosonic irreducible self-energies $\Sigma(K)$ and $\Phi(P)$ using the FRG, it is instructive to rederive the GM result for the critical temperature using the effective field theory derived above. Therefore it is convenient to start from formally exact skeleton equations (also called Dyson-Schwinger equations), which allow us to express the self-energies in terms of the induced interaction $\Gamma^{\bar{c}_\uparrow \bar{c}_\downarrow c_\downarrow c_\uparrow}(K'_1, K'_2; K_2, K_1)$ between fermions with oppo-

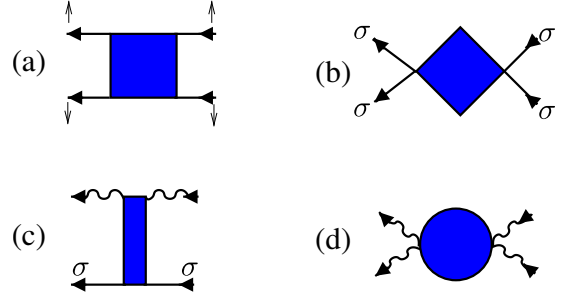


FIG. 3. Induced two-body interactions in our model system with bare action given in Eq. (2.3). (a) Induced interaction between fermions with opposite spin; (b) Induced interaction between fermions with parallel spin $\sigma = \uparrow, \downarrow$; the fact that the incoming and outgoing legs end at the same point on the vertex represents the antisymmetry of this vertex with respect to the exchange of the corresponding external labels. (c) Induced mixed fermion-boson interaction. (d) Induced two-body interaction between superfluid fluctuations; again, the symmetry of this vertex with respect to the exchange of the labels associated with the two incoming or outgoing legs is represented by the attachment of the legs to the same point on the vertex.

site spin. Graphically, the skeleton equations for the self-energies $\Sigma(K)$ and $\Phi(P)$ and for the irreducible three-point vertices $\Gamma^{\bar{c}_\uparrow \bar{c}_\downarrow c_\downarrow c_\uparrow}(K'_1, K'_2; P)$ and $\Gamma^{c_\downarrow c_\uparrow \bar{\psi}}(K'_1, K'_2; P)$ are shown in in Fig. 4. Formally, these equations can be derived by using the invariance of the functional integral representing the generating functional of the irreducible vertices under shift transformations of the fields.^{17,26} Explicitly, the skeleton equations relating the fermionic and bosonic self-energies to the three-point vertices are

$$\begin{aligned} \Sigma(K) &= - \int_P F(P)G(P-K)\Gamma^{\bar{c}_\uparrow \bar{c}_\downarrow c_\downarrow c_\uparrow}(K, P-K; P), \\ &= - \int_P \Gamma^{c_\downarrow c_\uparrow \bar{\psi}}(P-K, K; P)F(P)G(P-K), \end{aligned} \quad (2.9)$$

$$\begin{aligned} \Phi(P) &= \int_K G(K)G(P-K)\Gamma^{c_\downarrow c_\uparrow \bar{\psi}}(P-K, K; P) \\ &= \int_K \Gamma^{\bar{c}_\uparrow \bar{c}_\downarrow c_\downarrow c_\uparrow}(K, P-K; P)G(K)G(P-K), \end{aligned} \quad (2.10)$$

while the skeleton equations (c) and (d) in Fig. 4 relating the three-point vertex to the effective interaction between two fermions with opposite spin are

$$\begin{aligned} \Gamma^{\bar{c}_\uparrow \bar{c}_\downarrow c_\downarrow c_\uparrow}(K_1, K_2; P) &= 1 - \int_K G(K)G(P-K) \\ &\times \Gamma^{\bar{c}_\uparrow \bar{c}_\downarrow c_\downarrow c_\uparrow}(K_1, K_2; K, P-K), \end{aligned} \quad (2.11)$$

$$\begin{aligned} \Gamma^{c_\downarrow c_\uparrow \bar{\psi}}(K_1, K_2; P) &= 1 - \int_K G(K)G(P-K) \\ &\times \Gamma^{\bar{c}_\uparrow \bar{c}_\downarrow c_\downarrow c_\uparrow}(K, P-K; K_1, K_2). \end{aligned} \quad (2.12)$$

Substituting these expressions into Eqs. (2.10), we obtain the skeleton equation for the bosonic self-energy shown

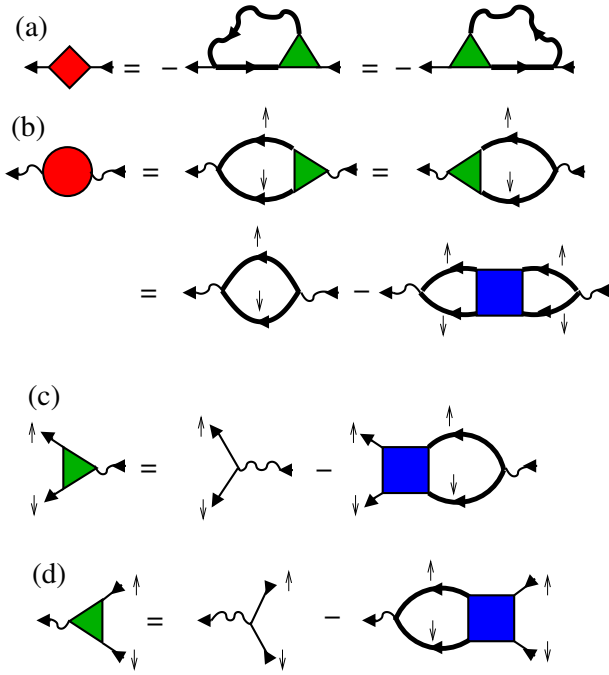


FIG. 4. The skeleton equation (a) expresses the exact fermionic self-energy $\Sigma(K)$ in terms of the exact three-point vertices $\Gamma^{\bar{c}_\uparrow c_\downarrow \psi}(K'_1, K'_2; P)$ and $\Gamma^{c_\downarrow c_\uparrow \bar{\psi}}(K'_1, K'_2; P)$ which are represented by green shaded triangles. In (b) we show three different ways of expressing the exact self-energy $\Phi(P)$ associated with the superfluid order parameter in terms of the three-point vertices or in terms of the exact effective interaction $\Gamma^{\bar{c}_\uparrow \bar{c}_\downarrow c_\downarrow c_\uparrow}(K'_1, K'_2; K_2, K_1)$ between two fermions with opposite spin. (c) and (d) represent skeleton equations relating the three-point vertices in terms of the effective interaction.

in the second line of Fig. 4 (b),

$$\begin{aligned} \Phi(P) &= \int_K G(K)G(P-K) \\ &\quad - \int_K \int_{K'} G(K)G(P-K)G(K')G(P-K') \\ &\quad \times \Gamma^{\bar{c}_\uparrow \bar{c}_\downarrow c_\downarrow c_\uparrow}(K, P-K; K', P-K'). \end{aligned} \quad (2.13)$$

C. Perturbative expansion in powers of the scattering length

The GM correction to the critical temperature can now be obtained by expanding the induced interaction between electrons with opposite spin appearing in the skeleton equation (2.13) to second order in the scattering length. Recall that in three dimensions the s -wave scattering length a_s is defined by

$$g = \frac{4\pi a_s}{m}, \quad (2.14)$$

where the so-called T -matrix in vacuum at vanishing total momentum is related to the bare interaction via

$$g^{-1} = g_0^{-1} - \Phi_0^{\text{vac}}(0), \quad (2.15)$$

and the particle-particle bubble at vanishing temperature and chemical potential is in three dimensions given by

$$\Phi_0^{\text{vac}}(0) = \int_{\mathbf{k}} \frac{\Theta(\Lambda_0 - |\mathbf{k}|)}{2\epsilon_{\mathbf{k}}} = \nu \frac{\Lambda_0}{k_F}. \quad (2.16)$$

Here Λ_0 is an ultraviolet cutoff in momentum space and

$$\nu = mk_F/(2\pi^2) \quad (2.17)$$

is the density of states (per spin projection) at the Fermi energy, where k_F is the Fermi momentum. To generate an expansion in powers of g , let us write the propagator of the pairing field in Gaussian approximation (where the bosonic self-energy is approximated by $\Phi(P) \approx \Phi_0(P)$, see Eq. (2.7)) in the following form

$$F_0(P) = \frac{1}{g_0^{-1} - \Phi_0(P)} = \frac{1}{g_0^{-1} - \Phi_0^{\text{reg}}(P)}, \quad (2.18)$$

where the regularized particle-particle bubble is

$$\Phi_0^{\text{reg}}(P) = \Phi_0(P) - \Phi_0^{\text{vac}}(0). \quad (2.19)$$

Due to the subtraction this expression is ultraviolet convergent so that we may take the limit $\Lambda_0 \rightarrow \infty$. Assuming $|g| \ll 1$ and that the relevant momenta in loop integrations are such that $|g\Phi_0^{\text{reg}}(P)| \ll 1$ we may approximate

$$F_0(P) \approx g + \mathcal{O}(g^2). \quad (2.20)$$

The leading terms in the expansion of the fermionic self-energy and the effective interaction between fermions with opposite spin are shown in Fig. 5 (a) and (b). Explicitly, the first order self-energy correction in Fig. 5 (a) is

$$\Sigma_1 = -g \int_K G_0(K) = -g\rho_0, \quad (2.21)$$

where $\rho_0 = \int_K G_0(K)$ is the density (per spin projection) in the non-interacting limit. The induced interaction between fermions with opposite spin to order g^2 shown in Fig. 5 (b) can be written as

$$\Gamma^{\bar{c}_\uparrow \bar{c}_\downarrow c_\downarrow c_\uparrow}(K'_1, K'_2; K_2, K_1) \approx -g^2 \Pi_0(K'_1 - K_2), \quad (2.22)$$

where

$$\Pi_0(Q) = \int_K G_0(K)G_0(K-Q) \quad (2.23)$$

is the non-interacting particle-hole bubble. Substituting these expansions into the skeleton equation (2.13) for the bosonic self-energy we obtain the expansion shown in Fig. 5 (c), which can be written as

$$\Phi(P) = \Phi_0(P) + \Phi_1(P) + \Phi_2(P) + \dots, \quad (2.24)$$

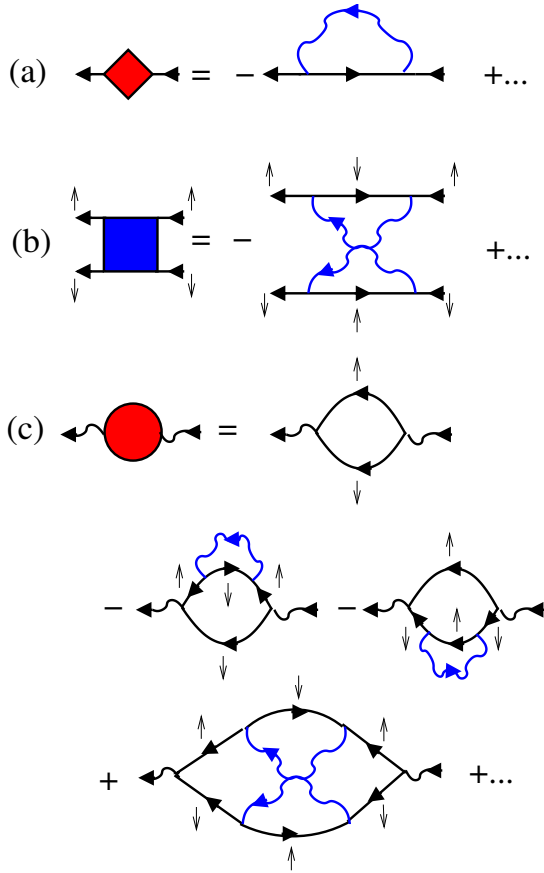


FIG. 5. Perturbative expansion in powers of the T -matrix g which is represented by a blue wavy arrow. (a) Fermionic self-energy, (b) induced interaction between two fermions with opposite spin, and (c) bosonic self-energy.

where the non-interacting particle-particle bubble $\Phi_0(P)$ is given in Eq. (2.7), the first order correction is

$$\Phi_1(P) = -2g\rho_0 \int_K G_0^2(K)G_0(P-K), \quad (2.25)$$

while the leading correction due to the induced interaction is

$$\Phi_2(P) = g^2 \int_K \int_{K'} G_0(K)G_0(P-K) \times \Pi_0(K-K')G_0(K')G_0(P-K'). \quad (2.26)$$

If we follow GM¹⁰ and work at constant density, the self-energy Σ_1 is exactly canceled by a shift in the chemical potential which is necessary to keep the density fixed; in this case we should ignore the first order correction $\Phi_1(P)$, so that the leading interaction correction to $\Phi(P)$ is given by the second order term $\Phi_2(P)$. On the other hand, at constant chemical potential the term $\Phi_1(P)$ modifies the GM result.

According to Eq. (2.8), the critical temperature is determined by

$$0 = g_0^{-1} - \Phi(0) \approx g^{-1} - \Phi_0^{\text{reg}}(0) - \Phi_1(0) - \Phi_2(0). \quad (2.27)$$

An explicit evaluation of the three contributions on the right-hand side of this equation in the BCS regime (where $\mu \approx E_F$) is given in Appendix A. Here we briefly summarize the main results. First of all, for temperatures $T \ll E_F$ the regularized particle-particle bubble is given by

$$\Phi_0^{\text{reg}}(0) = \nu [\ln(A/\tau) + \mathcal{O}(\tau)], \quad (2.28)$$

where $\tau = T/E_F$ and

$$A = \frac{8}{\pi e^{2-\gamma_E}}. \quad (2.29)$$

Here $\gamma_E = 0.577\dots$ is the Euler-Mascheroni constant. If we ignore the terms $\Phi_1(0)$ and $\Phi_2(0)$ on the right-hand side of Eq. (2.27) we obtain the mean-field critical temperature

$$\frac{T_{c0}}{E_F} = \tau_{c0} = Ae^{-1/\tilde{g}} = \frac{8e^{\gamma_E}}{\pi e^2} e^{-1/\tilde{g}}, \quad (2.30)$$

with the dimensionless interaction constant

$$\tilde{g} = \nu g = \frac{2}{\pi} k_F a_s. \quad (2.31)$$

As shown in Appendix A, for $P = 0$ the first order correction to the particle-particle bubble (2.25) is at low temperatures given by

$$\Phi_1(0) = \alpha_1 g \nu^2 [\ln(A/\tau) + \lambda_0], \quad (2.32)$$

where

$$\alpha_1 = 1/3, \quad (2.33)$$

and $\lambda_0 = \Lambda_0/k_F$ is a dimensionless ultraviolet cutoff which is necessary to regularize the relevant momentum integral. As discussed above, the contribution $\Phi_1(0)$ should be omitted if we work at constant density. The second order correction to the particle-particle bubble is

$$\Phi_2(0) = \alpha_2 g^2 \nu^3 [\ln(A/\tau) + \lambda_0]^2, \quad (2.34)$$

with

$$\alpha_2 = -\frac{1 + \ln 4}{3}. \quad (2.35)$$

Consider first the case of constant density, where the contribution from $\Phi_1(0)$ should be omitted. Substituting Eqs. (2.28) and (2.34) into Eq. (2.27) we obtain the following estimate of the dimensionless critical temperature,

$$\tau_c = Ae^{\alpha_2} e^{-1/\tilde{g}} \times [1 + \mathcal{O}(\tilde{g}\lambda_0)]. \quad (2.36)$$

In the asymptotic weak coupling limit $\tilde{g}\lambda_0 \ll 1$ we may neglect the cutoff-dependent correction and find that the induced interaction due to particle-hole fluctuations reduces the critical temperature for superfluidity by a factor of

$$\frac{T_c}{T_{c0}} = e^{\alpha_2} = \frac{1}{(4e)^{1/3}} \approx 0.451, \quad (2.37)$$

in agreement with GM.¹⁰ Note that according to Eq. (2.36) the cutoff-dependent correction to the GM result is of the order $\hat{g}\Lambda_0 = \nu g\Lambda_0/k_F$ which depends linearly on the ultraviolet cutoff Λ_0 . We show in Appendix A that this linear cutoff dependence is an artifact of neglecting the momentum- and frequency dependence of the particle-hole bubble $\Pi_0(K - K')$ in the evaluation of Eq. (2.26). In a more accurate calculation taking the momentum or the frequency dependence of $\Pi_0(K - K')$ into account the correction depends only logarithmically on the cutoff. If the chemical potential is held constant, then the term $\Phi_1(0)$ is not canceled and we obtain

$$\frac{T_c}{T_{c0}} = e^{\alpha_1 + \alpha_2} = \frac{1}{4^{1/3}} \approx 0.630 \quad \text{for constant } \mu, \quad (2.38)$$

which is larger than the GM result in Eq. (2.37). The discrepancy to the GM result for T_c found in a recent renormalization group calculation by Tanizaki *et al.*²⁰ seems to be due to the fact that these authors did not fix the density in their calculation.

III. INDUCED INTERACTIONS AND VERTEX CORRECTIONS FROM THE FRG

In order to understand the origin of the GM correction from the renormalization group point of view and to set up a machinery which allows us to calculate the fermionic self-energy non-perturbatively, we develop in this section

a general FRG approach for our model with bare action given by Eq. (2.3). To derive formally exact FRG flow equations for the irreducible vertices of our model, we introduce an additional cutoff Λ such that for large Λ fluctuations are suppressed while for $\Lambda \rightarrow 0$ we obtain our original model.¹⁷ The evolution of the generating functional of the one-line irreducible vertices under changes of the cutoff is described by the Wetterich equation.²⁷ By expanding this equation in powers of the fields, we obtain a formally exact hierarchy of FRG flow equations for all one-line irreducible vertices of our theory. For the implementation of this procedure there is considerable freedom in the choice of the cutoff scheme. For our purpose it is most convenient to use the particle-particle version of the momentum-transfer cutoff scheme proposed in Refs. [28 and 29], which has been shown to be useful in several other contexts.^{17,30,31} In this *interaction-momentum cutoff scheme*, we replace the inverse bare coupling g_0^{-1} of our model by the cutoff- and momentum-dependent coupling

$$g_{0,\Lambda}^{-1}(\mathbf{p}) = g_0^{-1} + R_\Lambda(\mathbf{p}), \quad (3.1)$$

there the regulator function vanishes for $\Lambda \rightarrow 0$ and approaches some large value for $\Lambda \rightarrow \Lambda_0$, where Λ_0 is some large initial value of the cutoff. Below we will work with a sharp momentum cutoff which amounts to setting

$$g_{0,\Lambda}(\mathbf{p}) = g_0\Theta(|\mathbf{p}| - \Lambda). \quad (3.2)$$

For $\Lambda < \Lambda_0$, the generating functional of the cutoff-dependent one-particle irreducible vertices of our model can be expanded in powers of the fields as follows

$$\begin{aligned} \Gamma_\Lambda[\bar{c}, c, \bar{\psi}, \psi] &= \int_K \sum_\sigma \Sigma_\Lambda(K) \bar{c}_{K\sigma} c_{K\sigma} - \int_P \Phi_\Lambda(P) \bar{\psi}_P \psi_P \\ &+ \int_K \int_P \left[\Gamma_\Lambda^{\bar{c}_\uparrow \bar{c}_\downarrow \psi}(K+P, -K; P) \bar{c}_{K+P\uparrow} \bar{c}_{-K\downarrow} \psi_P + \Gamma_\Lambda^{c_\downarrow c_\uparrow \bar{\psi}}(-K, K+P; P) c_{-K\downarrow} c_{K+P\uparrow} \bar{\psi}_P \right] \\ &+ \int_{K'_1} \int_{K'_2} \int_{K_2} \int_{K_1} \delta_{K'_1+K'_2, K_2+K_1} \Gamma_\Lambda^{\bar{c}_\uparrow \bar{c}_\downarrow c_\downarrow c_\uparrow}(K'_1, K'_2; K_2, K_1) \bar{c}_{K'_1\uparrow} \bar{c}_{K'_2\downarrow} c_{K_2\downarrow} c_{K_1\uparrow} \\ &+ \frac{1}{(2!)^2} \int_{K'_1} \int_{K'_2} \int_{K_2} \int_{K_1} \sum_\sigma \delta_{K'_1+K'_2, K_2+K_1} \Gamma_\Lambda^{\bar{c}_\sigma c_\sigma c_\sigma}(K'_1, K'_2; K_2, K_1) \bar{c}_{K'_1\sigma} \bar{c}_{K'_2\sigma} c_{K_2\sigma} c_{K_1\sigma} \\ &+ \int_{K'} \int_K \int_{P'} \int_P \sum_\sigma \delta_{K'+P', K+P} \Gamma_\Lambda^{\bar{c}_\sigma c_\sigma \bar{\psi} \psi}(K', K; P', P) \bar{c}_{K'\sigma} c_{K\sigma} \bar{\psi}_{P'} \psi_P \\ &+ \frac{1}{(2!)^2} \int_{P'_1} \int_{P'_2} \int_{P_2} \int_{P_1} \delta_{P'_1+P'_2, P_2+P_1} \Gamma_\Lambda^{\bar{\psi} \bar{\psi} \psi \psi}(P'_1, P'_2; P_2, P_1) \bar{\psi}_{P'_1} \bar{\psi}_{P'_2} \psi_{P_2} \psi_{P_1} + \dots, \end{aligned} \quad (3.3)$$

where the ellipsis represents terms involving five and more powers of the fields and all vertices are assumed to be properly symmetrized with respect to permutations of the labels associated with fields of the same type. $\Sigma_\Lambda(K)$ and $\Phi_\Lambda(P)$ are the cutoff-dependent fermionic and bosonic irreducible self-energies. The corresponding

cutoff-dependent inverse propagators are

$$G_\Lambda^{-1}(K) = G_{0,\Lambda}^{-1}(K) - \Sigma_\Lambda(K), \quad (3.4)$$

$$F_\Lambda^{-1}(P) = g_{0,\Lambda}^{-1}(\mathbf{p}) - \Phi_\Lambda(P). \quad (3.5)$$

The last four lines in Eq. (3.3) represent the various induced interactions shown graphically in Fig. 3. Although

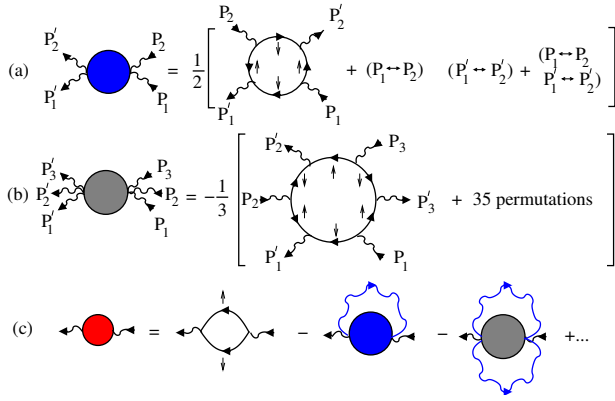


FIG. 6. (a) and (b) represent the vertices with four and six bosonic external legs at the initial cutoff $\Lambda = \Lambda_0$ in our cutoff scheme where only the bosonic propagator is regularized. In (c) we show the perturbative expansion of the bosonic self-energy in powers of the T -matrix g in vacuum (blue wavy arrows), which is obtained by approximating the Gaussian propagators of the order parameter field by $F_0(P) \approx g$. The one-loop contraction of the four-point vertex contains the self-energy corrections to the particle-particle bubble shown in Fig. 5 (c), while the two-loop contraction of the six-point vertex contains the GM correction shown in the last line of Fig. 5 (c). The minus signs in (c) are due to the fact that in Eq. (3.3) there is a relative minus sign between $\Phi_\Lambda(P)$ and the other vertices.

these interactions do not appear in our bare action given in Eq. (2.3), they are generated by the FRG flow. Since we do not introduce the regulator into the fermionic sector of our model, we have to start the FRG flow at some large initial scale $\Lambda = \Lambda_0$ with a non-trivial initial condition, as explained in Refs. 17 and 29. Hence, apart from the initial values of the three-legged vertices which appear in the bare action (2.3),

$$\Gamma_{\Lambda_0}^{\bar{c}_\uparrow \bar{c}_\downarrow \psi}(K+P, -K; P) = \Gamma_{\Lambda_0}^{c_\downarrow c_\uparrow \bar{\psi}}(-K, K+P; P) = 1, \quad (3.6)$$

all purely bosonic $2n$ -point vertices with n incoming and n outgoing boson lines are finite at the initial cutoff Λ_0 . Diagrammatically, these vertices can be identified with the symmetrized closed fermion loops with n incoming and n outgoing external bosonic legs, as shown in Fig. 6. Specifically, the initial value of the bosonic self-energy is the non-interacting particle-particle bubble,

$$\Phi_{\Lambda_0}(P) = \Phi_0(P) = \int_K G_0(K)G_0(P-K), \quad (3.7)$$

while the bosonic four-point vertex at the initial cutoff scale is

$$\begin{aligned} \Gamma_{\Lambda_0}^{\bar{\psi} \bar{\psi} \psi \psi}(P_1', P_2'; P_2, P_1) &= \frac{1}{2} \int_K \left[G_0(K)G_0(-K+P_1') \right. \\ &\times G_0(K-P_1'+P_2)G_0(-K+P_1'-P_2+P_2') \\ &\left. + (P_1 \leftrightarrow P_2) + (P_1' \leftrightarrow P_2') + (P_1 \leftrightarrow P_2, P_1' \leftrightarrow P_2') \right]. \end{aligned} \quad (3.8)$$

Note that this vertex is symmetric with respect to the independent exchange $P_1' \leftrightarrow P_2'$ and $P_1 \leftrightarrow P_2$. Setting all external momenta and frequencies equal to zero we obtain

$$\Gamma_{\Lambda_0}^{\bar{\psi} \bar{\psi} \psi \psi}(0) = \frac{7\zeta(3)}{4} \frac{\nu}{(\pi T)^2}. \quad (3.9)$$

The contribution of the higher order bosonic vertices to the initial value of the generating functional (3.3) is

$$\begin{aligned} \Gamma_{\Lambda_0}^{n>3}[\bar{\psi}, \psi] &= \sum_{n=3}^{\infty} \frac{1}{(n!)^2} \int_{P_1'} \cdots \int_{P_n'} \int_{P_n} \cdots \int_{P_1} \\ &\times \delta_{P_1'+\dots+P_n', P_n+\dots+P_1} \Gamma_{\Lambda_0}^{(2n)}(P_1', \dots, P_n'; P_n, \dots, P_1) \\ &\times \bar{\psi}_{P_1'} \cdots \bar{\psi}_{P_n'} \psi_{P_n} \cdots \psi_{P_1}. \end{aligned} \quad (3.10)$$

In our approach the GM correction to T_c is determined by the initial value of the bosonic six-point vertex, which after symmetrization can be written as

$$\begin{aligned} \Gamma_{\Lambda_0}^{(6)}(P_1', P_2', P_3'; P_3, P_2, P_1) &= \\ &-\frac{1}{3} \int_K \left[G_0(K)G_0(-K+P_1')G_0(K-P_1'+P_2) \right. \\ &\times G_0(-K+P_1'-P_2+P_2')G_0(K-P_1'+P_2-P_2'+P_3) \\ &\times G_0(-K+P_1'-P_2+P_2'-P_3+P_3') \\ &\left. + (3!)^2 - 1 \text{ permutations of } (P_1', P_2', P_3') \text{ and } (P_1, P_2, P_3) \right]. \end{aligned} \quad (3.11)$$

All other vertices vanish at the initial scale, but all vertices which are compatible with the $U(1)$ -symmetry of the bare action are generated by the FRG flow, in particular the induced interactions shown in Fig. 3. From the bosonic sector of our initial action $\Gamma_{\Lambda_0}[\bar{c}, c, \bar{\psi}, \psi]$ it is easy to reproduce the perturbation series for the renormalized particle-particle bubble shown graphically in Fig. 5 (c). The non-interacting particle-particle bubble is contained in the Gaussian propagator $F_0(P) = [g_0^{-1} - \Phi_0(P)]^{-1}$, see Eq. (2.18). The first order corrections shown in the second line of Fig. 5 (c) can be recovered from the one-loop contraction of the four-point vertex shown in Fig. 6 (c), while the last diagram in Fig. 5 (c) which gives the GM correction is contained in the two-loop contraction of the six-point vertex shown in Fig. 6 (c).

Let us now write down exact FRG flow equations for the self-energies of our model in our interaction-momentum cutoff scheme. The derivation of these flow equations is straightforward following the general procedure outlined in Ref. [17]. The cutoff-dependent fermionic self-energy satisfies

$$\begin{aligned} \partial_\Lambda \Sigma_\Lambda(K) &= \int_P \dot{F}_\Lambda(P) \Gamma_\Lambda^{\bar{c}_\sigma c_\sigma \bar{\psi} \psi}(K; K; P; P) \\ &- \int_P \dot{F}_\Lambda(P) G_\Lambda(P-K) \Gamma_\Lambda^{\bar{c}_\uparrow \bar{c}_\downarrow \psi}(K, P-K; P) \\ &\times \Gamma_\Lambda^{c_\downarrow c_\uparrow \bar{\psi}}(P-K, K; P), \end{aligned} \quad (3.12)$$

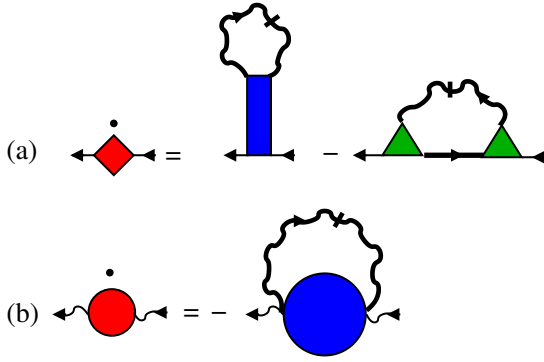


FIG. 7. Graphical representation of the exact FRG flow equations for (a) the fermionic and (b) the bosonic self-energy of our model using the interaction-momentum cutoff scheme, see Eqs. (3.12) and (3.13). The notations for the vertices and propagators are the same as in Figs. 2, 3 and 4. A dot over a vertex denotes the cutoff derivative and wavy arrows with an additional slash represent the bosonic single-scale propagator defined in Eq. (3.14).

while the flow of the bosonic self-energy (which can be

$$\begin{aligned} \partial_\Lambda \Gamma_\Lambda^{\bar{c}_\uparrow \bar{c}_\downarrow \psi} (K_1, K_2; P) &= \int_{P'} \dot{F}_\Lambda(P') \Gamma_\Lambda^{\bar{c}_\uparrow \bar{c}_\downarrow \bar{\psi} \psi \psi} (K_1, K_2; P'; P, P) \\ &+ \int_{P'} \dot{F}_\Lambda(P') G_\Lambda(P' - K_1) \Gamma_\Lambda^{\bar{c}_\uparrow \bar{c}_\downarrow \psi} (P' - K_1, K_1; P') \Gamma_\Lambda^{\bar{c}_\uparrow c_\uparrow \bar{\psi} \psi} (K_2; P' - K_1; P'; P) \\ &+ \int_{P'} \dot{F}_\Lambda(P') G_\Lambda(P' - K_2) \Gamma_\Lambda^{\bar{c}_\uparrow \bar{c}_\downarrow \psi} (K_2, P' - K_2; P') \Gamma_\Lambda^{\bar{c}_\downarrow c_\downarrow \bar{\psi} \psi} (K_1; P' - K_2; P'; P), \end{aligned} \quad (3.15)$$

$$\begin{aligned} \partial_\Lambda \Gamma_\Lambda^{c_\downarrow c_\uparrow \bar{\psi}} (K_1, K_2; P) &= \int_{P'} \dot{F}_\Lambda(P') \Gamma_\Lambda^{c_\downarrow c_\uparrow \bar{\psi} \bar{\psi} \psi} (K_1, K_2; P, P', P') \\ &+ \int_{P'} \dot{F}_\Lambda(P') G_\Lambda(P' - K_1) \Gamma_\Lambda^{c_\downarrow c_\uparrow \bar{\psi}} (K_1, P' - K_1; P') \Gamma_\Lambda^{\bar{c}_\uparrow c_\uparrow \bar{\psi} \psi} (P' - K_1; K_2; P'; P) \\ &+ \int_{P'} \dot{F}_\Lambda(P') G_\Lambda(P' - K_2) \Gamma_\Lambda^{c_\downarrow c_\uparrow \bar{\psi}} (P' - K_2, K_2; P') \Gamma_\Lambda^{\bar{c}_\downarrow c_\downarrow \bar{\psi} \psi} (P' - K_2; K_1; P'; P). \end{aligned} \quad (3.16)$$

A graphical representation of Eqs. (3.15) and (3.16) is shown in Fig. 8.

Next, consider the bosonic four-point vertex $\Gamma_\Lambda^{\bar{\psi} \bar{\psi} \psi \psi} (P'_1, P'_2; P_2, P_1)$ which controls the FRG flow of the bosonic self-energy in Eq. (3.13). Recall that in our interaction-momentum cutoff scheme this ver-

identified with the renormalized particle-particle bubble) is given by

$$\partial_\Lambda \Phi_\Lambda(P) = - \int_{P'} \dot{F}_\Lambda(P') \Gamma_\Lambda^{\bar{\psi} \bar{\psi} \psi \psi} (P, P'; P', P). \quad (3.13)$$

Here $\dot{F}_\Lambda(P)$ is the bosonic single-scale propagator, which for our sharp interaction-momentum cutoff scheme is simply given by

$$\dot{F}_\Lambda(P) = - \frac{\delta(p - \Lambda)}{g_0^{-1} - \Phi_\Lambda(P)}. \quad (3.14)$$

A graphical representation of Eqs. (3.12) and (3.13) is shown in Fig. 7.

Note that in our interaction-momentum cutoff scheme only diagrams with bosonic single-scale propagators appear in the flow equations. For this simplification we pay the price that we have to start the FRG flow with a non-trivial initial condition, as explained above.

The right-hand sides of the flow equations (3.12) and (3.13) for the self-energies depend on higher order vertices with three and four external legs for which we can derive again exact FRG flow equations. The flow equations for the three-point vertices are

tex, which describes the induced interaction between fluctuations of the superfluid order parameter, has a finite initial value at $\Lambda = \Lambda_0$ given by the symmetrized fermion loop in Eq. (3.8). The FRG flow equation for the bosonic four-point vertex is (see Fig. 9)

$$\begin{aligned} \partial_\Lambda \Gamma_\Lambda^{\bar{\psi} \bar{\psi} \psi \psi} (P'_1, P'_2; P_2, P_1) &= \int_P \dot{F}_\Lambda(P) \Gamma_\Lambda^{(6)} (P'_1, P'_2, P'; P', P_2, P_1) \\ &- \int_P \dot{F}_\Lambda(P) F_\Lambda(P_1 + P_2 - P) \Gamma_\Lambda^{\bar{\psi} \bar{\psi} \psi \psi} (P'_1, P'_2; P_1 + P_2 - P, P) \Gamma_\Lambda^{\bar{\psi} \bar{\psi} \psi \psi} (P, P_1 + P_2 - P; P_2, P_1) \\ &- \int_P [F_\Lambda(P) F_\Lambda(P + P_1 - P'_1)] \bullet \Gamma_\Lambda^{\bar{\psi} \bar{\psi} \psi \psi} (P'_1, P + P_1 - P'_1; P, P_1) \Gamma_\Lambda^{\bar{\psi} \bar{\psi} \psi \psi} (P'_2, P; P + P_1 - P'_1, P_2) \end{aligned}$$

$$- \int_P [F_\Lambda(P)F_\Lambda(P + P_2 - P'_1)]^\bullet \Gamma_\Lambda^{\bar{\psi}\bar{\psi}\psi\psi}(P'_1, P + P_2 - P'_1; P, P_2) \Gamma_\Lambda^{\bar{\psi}\bar{\psi}\psi\psi}(P'_2, P; P + P_2 - P'_1, P_1), \quad (3.17)$$

where we have introduced the following product rule notation,

$$[F_\Lambda(P)F_\Lambda(P')]^\bullet = \dot{F}_\Lambda(P)F_\Lambda(P') + F_\Lambda(P)\dot{F}_\Lambda(P'). \quad (3.18)$$

To conclude this section, let us briefly discuss the flow equations of the induced interactions which vanish at the initial cutoff scale: the mixed fermion-boson vertex $\Gamma_\Lambda^{\bar{c}_\sigma c_\sigma \bar{\psi}\psi}$ and the induced fermionic interactions $\Gamma_\Lambda^{\bar{c}_\uparrow \bar{c}_\downarrow c_\downarrow c_\uparrow}$ and $\Gamma_\Lambda^{\bar{c}_\sigma \bar{c}_\sigma c_\sigma c_\sigma}$ which appear in the vertex expansion (3.3) and are represented by the symbols defined in Fig. 3 (a) and (b). The exact FRG flow equations for these vertices are rather complicated and are given in Appendix B. Because the right-hand sides of the flow equations for the mixed fermion-boson vertex $\Gamma_\Lambda^{\bar{c}_\sigma c_\sigma \bar{\psi}\psi}$ and for the fermionic interaction vertex $\Gamma_\Lambda^{\bar{c}_\uparrow \bar{c}_\downarrow c_\downarrow c_\uparrow}$ are finite even if the above four-point vertices are neglected, the FRG flow generates finite values of these induced interactions. An approximate method to take these induced interactions into account is to retain only those vertices in the FRG flow equations which are finite at the initial scale. In Ref. 31 we have obtained reasonable results using a similar strategy to truncate the hierarchy of FRG flow equations for the vertices in a low-energy model for graphene. Following this strategy, we arrive to the simplified FRG flow equations for the induced interactions

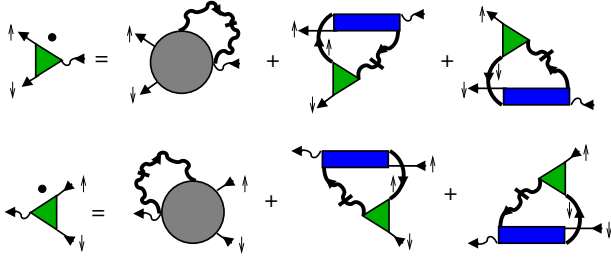


FIG. 8. Graphical representation of the exact FRG flow equations (3.15) and (3.16) for the three-point vertices.

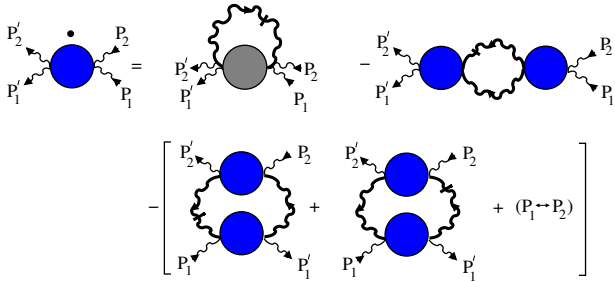


FIG. 9. Graphical representation of the exact FRG flow equation (3.17) for the induced interaction between pairing fluctuations.

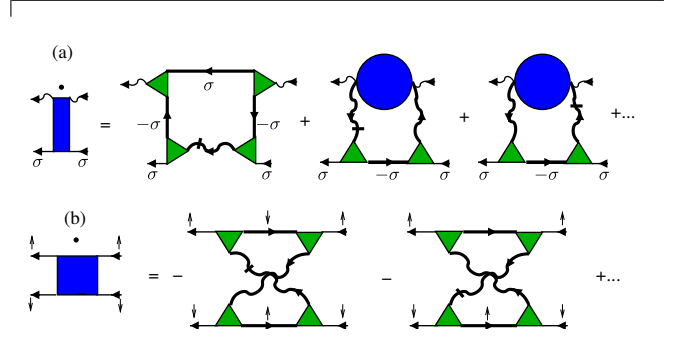


FIG. 10. Approximate FRG flow equations for the induced interactions in a truncation where only those vertices are retained on the right-hand side which are finite at the initial cutoff scale: (a) mixed fermion-boson vertex; (b) interaction vertex between two fermions with opposite spin.

shown graphically in Fig. 10. Note that the induced interaction between fermions with parallel spin still vanishes within this approximation.

In Appendix E we present an approximate evaluation of the flow equation for the mixed four-point vertex shown in Fig. 10 (a) and study the effect of this vertex on the fermionic self-energy. At this point, let us make three comments on the truncated flow equations of the induced interactions shown in Fig. 10. First of all, if we replace the boson propagators in the approximate flow equation for the fermionic interaction vertex shown in Fig. 10 (b) by the T -matrix g and neglect all self-energy corrections to the fermionic propagators, we recover the leading term in the perturbative expansion of this interaction vertex shown in Fig. 5 (b). Note, however, that within our interaction-momentum cutoff scheme this vertex does not directly couple to the FRG flow of the bosonic self-energy. The corresponding renormalization of the critical temperature is taken into account via the bosonic six-point vertex, as explained in the text after Eq. (3.11).

Next, we note that for small values of the scattering matrix g we can use these flow equations to calculate higher order vertex corrections to various physical quantities. For example, from the truncated flow equation for the mixed fermion-boson vertex shown in Fig. 10 (a) it is obvious that this vertex is at least of order g . From the exact flow equations for the three-point vertices shown in Fig. 8 we then see that the latter are at least of order g^2 .

Finally, let us point out that the induced interactions can exhibit some rather complicated momentum- and frequency dependence. Only in cases where this can be neglected, one can try to avoid the appearance of the induced interactions by redefining the bosonic Hubbard-Stratonovich fields ψ and $\bar{\psi}$. This strategy, which has been called dynamical re-bosonization,³² was adopted by

Floerchinger *et al.*¹³ who attempted to reproduce the GM correction to the critical temperature using this strategy. However, the numerical value of the GM correction is determined by the full momentum dependence of the induced interaction in (B5), so that it is not surprising that Floerchinger *et al.*¹³ could not reproduce the precise numerical value of the GM correction given in Eq. (2.37).

IV. DENSITY OF STATES AND QUASIPARTICLE DAMPING IN THE NORMAL STATE CLOSE TO T_c

In this section, we shall consider the effect of superfluid fluctuations on the electronic self-energy in the normal state at and slightly above the critical temperature. This effect is usually neglected,¹ which is only correct for temperatures not too close to T_c . Surprisingly, a quantitatively accurate calculation of the electronic self-energy in this regime cannot be found in the literature. Although such a theory is currently needed in other contexts, e.g. temporal development of an order parameter following a sudden quench in the field of out-of-equilibrium dynamics.^{33–35} To begin with, we analyze this problem in Sec. IV A within the Gaussian approximation for the propagator of the superfluid order parameter field. However, the critical behavior of the superfluid order parameter belongs to the XY-universality class, which below four dimensions is controlled by the Wilson-Fisher fixed point. In Sec. IV B we shall therefore present a more accurate analysis of this problem using the FRG approach developed in Sec. III.

A. Gaussian approximation

To begin with, let us calculate the electronic self-energy within the Gaussian approximation, which is equivalent to calculating the effective interaction in ladder approximation. In the normal state the self-energy is then given by

$$\Sigma_1(K) = - \int_P F_0(P)G_0(P-K), \quad (4.1)$$

where the Gaussian propagator of the pairing field is given in Eq. (2.18). Since we are interested in the effect of long-wavelength and low-energy order parameter fluctuations on the fermionic self-energy, we may expand the inverse Gaussian propagator to leading order in momenta and frequencies,

$$F_0^{-1}(\mathbf{p}, i\bar{\omega}) = g^{-1} - \Phi_0^{\text{reg}}(\mathbf{p}, i\bar{\omega}) \approx \nu[t_0 + p^2/p_0^2 + |\bar{\omega}|/\omega_0]. \quad (4.2)$$

In the BCS regime and for $|T - T_{c0}| \ll T_{c0}$ the dimensionless parameter t_0 can be identified with the reduced temperature

$$t_0 = \frac{T - T_{c0}}{T_{c0}}, \quad (4.3)$$

while the momentum scale p_0 and the energy scale ω_0 are both proportional to the temperature¹

$$p_0 = \sqrt{\frac{48}{7\zeta(3)} \frac{\pi T}{v_F}}, \quad (4.4)$$

$$\omega_0 = \frac{8T}{\pi}. \quad (4.5)$$

Note that $1/p_0 = \xi_0$ can be identified with the coherence length of a clean three-dimensional superconductor with isotropic Fermi surface.¹ The Ginzburg-Levanyuk number Gi introduced in Eq. (1.1) can be written as¹

$$Gi = \left(\frac{7\zeta(3)p_0^3}{64\pi^3\nu T_c} \right)^2 = \frac{27}{28\zeta(3)} \left(\frac{\pi T_c}{E_F} \right)^4. \quad (4.6)$$

On the other hand, in the strong coupling regime where νg is not small the coefficients in the long-wavelength expansion of $F_0^{-1}(\mathbf{p}, i\bar{\omega})$ have a more complicated dependence in T and μ , as discussed in Appendix C. In particular, at the unitary point $g^{-1} = 0$ the momentum scale p_0 is of the order of k_F while ω_0 is of order E_F . Note that the corresponding expressions given by Larkin and Varlamov¹ are only valid in the BCS limit $\nu g \ll 1$.

Let us now focus on the effect of classical long-wavelength fluctuations of the superfluid order parameter on the fermionic self-energy. Because in the vicinity of the critical temperature the dynamics of the order parameter is slow compared with the electron dynamics, it is then sufficient to retain only the contribution from the zeroth Matsubara frequency in Eq. (4.1). In Appendix D we present a formal justification of this approximation. The resulting critical contribution to the fermionic self-energy is

$$\Sigma_{\text{crit}}(\mathbf{k}, i\omega) = \frac{T}{\nu} \int_{\mathbf{p}} \frac{\Theta(p_0 - |\mathbf{p}|)}{t_0 + \mathbf{p}^2/p_0^2} \frac{1}{i\omega + \xi_{\mathbf{p}-\mathbf{k}}}, \quad (4.7)$$

where the cutoff $\Theta(p_0 - |\mathbf{p}|)$ takes into account the range of validity of our long-wavelength expansion (4.2). Eq. (4.7) can be evaluated analytically without further approximation, but the result is very complicated so that we do not present it here. In Fig. 11 we plot the corresponding renormalized density of states

$$\nu_{\text{crit}}(E_F + \omega) = -\frac{1}{\pi} \text{Im} \int_{\mathbf{k}} \frac{1}{\omega - \xi_{\mathbf{k}} - \Sigma_{\text{crit}}(\mathbf{k}, \omega + i0^+)}. \quad (4.8)$$

Obviously, for $T \rightarrow T_c$ classical pairing fluctuations give rise to a pronounced pseudogap in the density of states at the Fermi energy. This has already been noticed by Di Castro *et al.* in Ref. [6] within a perturbative approach which amounts to expanding the right-hand side of Eq. (4.8) to first order in the self-energy. With this approximation Di Castro *et al.* obtained for the density of states at the Fermi-energy⁶

$$\nu_{\text{pert}}(E_F) = \nu_0 \left[1 - \sqrt{\frac{3}{7\zeta(3)} \frac{(\pi T/E_F)^2}{\sqrt{t_0}}} \right]. \quad (4.9)$$

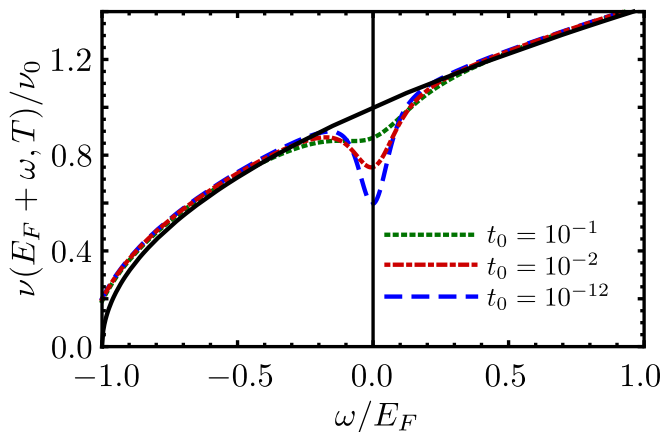


FIG. 11. Frequency-dependence of the modification of the density of states due to classical order parameter fluctuations obtained from the numerical evaluation of Eq. (4.8). The curves are for $T/E_F = 0.1$, $\mu = E_F$, and $t_0 = 10^{-1}$ (green dotted line), $t_0 = 10^{-2}$ (red dashed-dotted line), and $t_0 = 10^{-12}$ (blue dashed line). The solid black line is the non-interacting density of states $\nu(\epsilon)/\nu_0 = \sqrt{\epsilon/E_F}$.

This suppression of the density of states has been observed experimentally in the fluctuation regime above the superfluid transition of a strongly interacting Fermi gas.³⁶ However, for $t_0 \rightarrow 0$ the correction in Eq. (4.9) diverges. Clearly, this divergence is unphysical and signals the breakdown of perturbation theory for temperatures close to T_c . In contrast to the perturbative result (4.9) our expression (4.8) obtained within the Gaussian approximation predicts a finite suppression of the density of states for all $t_0 \geq 0$. To show this, we have evaluated Eq. (4.8) numerically for different temperatures. In Fig. 12. and show our numerical result for $\nu_{\text{crit}}(E_F)$ as a function of t_0 . Note that at the critical point $t_0 = 0$ the Gaussian approximation (4.8) predicts a finite suppression of the density of states at the Fermi energy.

The phenomenon that within perturbation theory superconducting fluctuations above T_c give rise to singular corrections to various physical quantities has first been noticed by Aslamazov and Larkin,⁵ who discovered a $1/t_0$ singularity in the conductivity of normal metals due to virtually formed Cooper pairs above T_c . Moreover, Maki³⁷ and Thompson³⁸ have shown that Cooper pair formation along diffusive paths in a disordered conductor also lead to singularities in the the transport coefficients. Although the Maki-Thompson correction to the conductivity has generally a weaker functional dependence on the reduced temperature t_0 , in certain regimes it can be larger than the Aslamazov-Larkin correction. However, similar to the singularity in the density of states given in Eq. (4.9), the perturbatively generated singularities at $T = T_c$ should be regularized by some higher order process. The only systematic way of introducing a cutoff at $T = T_c$ so far is an external pair-breaking mech-

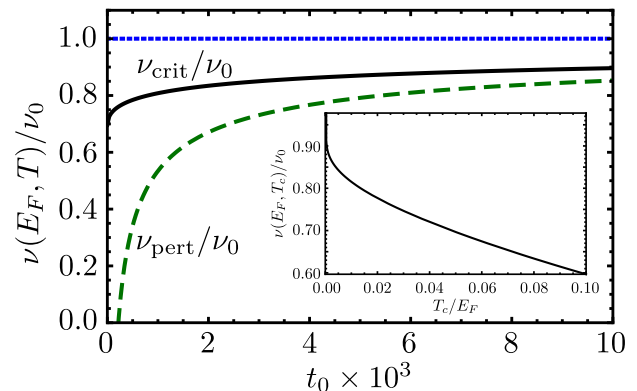


FIG. 12. The solid line represents our result (4.8) for the density of states at the Fermi energy $\nu_{\text{crit}}(E_F, T)$ as a function of the reduced temperature $t_0 = (T - T_{c0})/T_{c0}$ for $T_c/E_F = 0.05$. Note that for $t_0 \rightarrow 0$ the density of states has a finite limit. The green dashed line represents the perturbative result (4.9) derived by Di Castro *et al.*⁶ which diverges at the critical temperature as $-1/\sqrt{t_0}$. In the inset we show the behavior of $\nu_{\text{crit}}(E_F, T_{c0})$ as a function of T_{c0} .

anism, such as magnetic impurities or electron-phonon interactions.³⁹ There were a few attempts to identify a cutoff at T_c within the microscopic theory itself: by accounting for some subclasses of higher order diagrams⁴⁰ and by accounting for non-linear effects of the fluctuations through Gorkov equation,⁴¹ at least in dirty superconductors. But the results are still inconclusive. Here we focus on the singularity in the density of states and propose a new strategy to solve this long-standing problem using renormalization group methods. In fact, from Fig. 12 it is clear that the singularity in the perturbative result (4.9) can be removed if we do not expand the density of the states in powers of the self-energy but insert the perturbative self-energy into the Dyson equation and use Eq. (4.8) to calculate the density of states.

To gain a better analytical understanding of the low-energy behavior of the self-energy, let us simplify the integrand in Eq. (4.7) by setting $\mathbf{k} = \mathbf{k}_F + \mathbf{q}$ and assuming $|\mathbf{q}| \ll k_F$. We may then approximate $\xi_{\mathbf{p}-\mathbf{k}} \approx -\mathbf{v}_F \cdot (\mathbf{p} - \mathbf{q}) = \xi_{\mathbf{k}} - \mathbf{v}_F \cdot \mathbf{p}$. We have verified numerically that this approximation correctly reproduces the main low-energy features of the self-energy. After analytic continuation ($i\omega \rightarrow \omega + i0^+$) we obtain from Eq. (4.7) for the imaginary part for $t_0 \ll 1$ and $|\omega + \xi_{\mathbf{k}}| \ll v_F p_0$,

$$\text{Im}\Sigma_{\text{crit}}(\mathbf{k}, \omega + i0^+) = T \frac{p_0^2}{\nu v_F} \frac{\pi}{2} \ln \left[t_0 + \left(\frac{\omega + \xi_{\mathbf{k}}}{v_F p_0} \right)^2 \right]. \quad (4.10)$$

To calculate the real part of the self-energy for $t_0 \ll 1$ and $|\omega + \xi_{\mathbf{k}}| \ll v_F p_0$ we first perform the angular integration in Eq. (4.7) and obtain

$$\text{Re}\Sigma_{\text{crit}}(\mathbf{k}, \omega + i0^+) = T \frac{p_0^2}{\nu v_F} \text{sgn}(\omega + \xi_{\mathbf{k}})$$

$$\times \int_0^1 \frac{dx}{t_0 + x^2} \ln \left| \frac{x + \frac{|\omega + \xi_{\mathbf{k}}|}{v_F p_0}}{x - \frac{|\omega + \xi_{\mathbf{k}}|}{v_F p_0}} \right|. \quad (4.11)$$

In the regime $\sqrt{t_0} \ll |\omega + \xi_{\mathbf{k}}|/(v_F p_0) \ll 1$ we may set $t_0 = 0$ and move the upper limit of the x -integral to infinity. Using the fact that for $a > 0$,

$$\int_0^\infty \frac{dx}{x} \ln \left| \frac{x+a}{x-a} \right| = \frac{\pi^2}{2} \quad (4.12)$$

we obtain for $\sqrt{t_0} \ll |\omega + \xi_{\mathbf{k}}|/(v_F p_0) \ll 1$,

$$\text{Re}\Sigma_{\text{crit}}(\mathbf{k}, \omega + i0^+) \approx T \frac{p_0^2}{\nu v_F} \frac{\pi^2}{2} \text{sgn}(\omega + \xi_{\mathbf{k}}). \quad (4.13)$$

In the opposite regime $|\omega + \xi_{\mathbf{k}}|/(v_F p_0) \ll \sqrt{t_0} \ll 1$ we may expand the logarithm for $x \gg |\omega + \xi_{\mathbf{k}}|/(v_F p_0)$,

$$\ln \left| \frac{x + \frac{|\omega + \xi_{\mathbf{k}}|}{v_F p_0}}{x - \frac{|\omega + \xi_{\mathbf{k}}|}{v_F p_0}} \right| \approx \frac{2}{x} \frac{|\omega + \xi_{\mathbf{k}}|}{v_F p_0}. \quad (4.14)$$

Then we obtain to leading order

$$\text{Re}\Sigma_{\text{crit}}(\mathbf{k}, \omega + i0^+) \approx T \frac{p_0^2}{\nu v_F} \frac{\pi}{\sqrt{t_0}} \frac{\omega + \xi_{\mathbf{k}}}{v_F p_0}. \quad (4.15)$$

Note that in both regimes the imaginary part of the self-energy is parametrically larger than the real part, so that from now on we shall simply neglect the real part of the self-energy.

Our result (4.10) for the imaginary part of the self-energy due to classical fluctuations of the superfluid order parameter implies that for $T \rightarrow T_{c0}$ the damping of quasiparticles on the Fermi surface diverges as

$$\gamma_{\text{crit}} = -\text{Im}\Sigma_{\text{crit}}(\mathbf{k}_F, i0^+) = \frac{\pi T}{2} \frac{p_0^2}{\nu v_F} \ln \left(\frac{T_{c0}}{T - T_{c0}} \right). \quad (4.16)$$

While within the Gaussian approximation the density of states is finite, the quasiparticle damping exhibits an unphysical logarithmic singularity for $T \rightarrow T_c$. In the BCS regime the logarithm is multiplied by a small prefactor $T p_0^2 / \nu v_F \propto T^3 / E_F^2$, while in the vicinity of the unitary point where $p_0 \propto k_F$ the prefactor is linear in the temperature, such that

$$\gamma_{\text{crit}} \propto T. \quad (4.17)$$

Comparing the above γ_{crit} with the generic form of the quasiparticle damping in a three-dimensional Fermi liquid,

$$\gamma_{\text{FL}} = C_{\text{FL}} T^2 / E_F, \quad (4.18)$$

where the numerical constant C_{FL} is usually of the order of unity,^{42,43} we conclude that for $\ln(1/t_0) \gtrsim E_F/T$ the contribution from classical superconducting fluctuations to the quasiparticle damping dominates.

It turns out, however, that the logarithmic divergence in Eq. (4.16) is an artifact of the Gaussian approximation. Physically, it is clear that both the damping of the intermediate states as well as the existence of an anomalous dimension η of the superfluid order parameter field will smooth out this singularity. For example, to take into account the usual Fermi liquid damping (4.18) we should replace the free propagator in Eq. (4.1) by

$$G_1(K) = \frac{1}{i\omega - \xi_{\mathbf{k}} + i\gamma_{\text{FL}} \text{sgn}\omega}. \quad (4.19)$$

Then we obtain for $T \rightarrow T_{c0}$ instead of Eq. (4.16),

$$\gamma_{\text{crit}} = \frac{\pi T_{c0}}{2} \frac{p_0^2}{\nu v_F} \ln \left(\frac{v_F p_0}{\gamma_{\text{FL}}} \right), \quad (4.20)$$

which is proportional to $T_{c0}^3 \ln(E_F/T_{c0})$ in the BCS regime. A similar sub-leading non-analytic correction to the self-energy of three-dimensional Fermi liquids is also generated by short-range interactions.⁴⁴ Note, however, that Eq. (4.20) does not take into account that the anomalous dimension η of superfluid fluctuations at the critical point. Recall that critical behavior of the superconducting transition belong to the universality class of the classical XY-model which is characterized by a finite critical exponent (anomalous dimension) $\eta \approx 0.038$ in three dimensions [45]. The true static propagator of the order-parameter field at $T = T_c$ is therefore for small momenta \mathbf{p} of the form

$$F_*(\mathbf{p}, 0) \sim \frac{A_*}{\nu} \left(\frac{p_0}{p} \right)^{2-\eta}, \quad (4.21)$$

where A_* is a dimensionless constant. If we replace the Gaussian propagator in Eq. (4.7) by Eq. (4.21) we obtain for the self-energy at the critical point,

$$\Sigma_{\text{crit}}(\mathbf{k}, i\omega) \approx \frac{T}{\nu} \int_{\mathbf{p}} \left(\frac{p_0}{p} \right)^{2-\eta} \frac{A_* \Theta(p_0 - |\mathbf{p}|)}{i\omega + \xi_{\mathbf{p}-\mathbf{k}}}. \quad (4.22)$$

From this expression it is easy to show that

$$\gamma_{\text{crit}} \propto \frac{T}{\eta} \frac{p_0^2}{\pi v_F} \propto \frac{1}{\eta} \frac{T^3}{E_F^2}. \quad (4.23)$$

Due to the small value of η , the prefactor of the leading T^3 -behavior is unusually large. Of course, the above procedure is not satisfactory because it does not self-consistently take the interplay between critical fluctuations and quasiparticle damping of intermediate states into account. We shall address this problem below using the FRG. This allows us to consistently take into account the feedback of non-Gaussian critical order parameter fluctuations on the electronic properties, which provide an intrinsic cutoff of the logarithmic singularity in the quasiparticle damping encountered in Gaussian approximation, see Eq. (4.16).

B. FRG calculation of the quasiparticle damping

The exact FRG flow equation of the fermionic self-energy $\Sigma_\Lambda(K)$ is given in Eq. (3.12) and is shown graphically in Fig. 7 (a). This flow equation depends on the cutoff-dependent mixed fermion-boson interaction $\Gamma_\Lambda^{\bar{c}_\sigma c_\sigma \bar{\psi} \psi}$ and on the three-point vertices $\Gamma_\Lambda^{\bar{c}_\uparrow \bar{c}_\downarrow \psi}$ and $\Gamma_\Lambda^{c_\downarrow c_\uparrow \bar{\psi}}$. In this subsection we shall neglect all vertices which vanish at the initial cutoff scale within our cutoff scheme. In particular, we set the mixed fermion-boson interaction vertex equal to zero,

$$\Gamma_\Lambda^{\bar{c}_\sigma c_\sigma \bar{\psi} \psi} \approx 0. \quad (4.24)$$

From the exact FRG flow equations (3.15, 3.16) for the three-point vertices shown graphically in Fig. 8 it is obvious that in our interaction-momentum cutoff scheme this truncation is consistent with approximating the three-point vertices by their initial values,

$$\Gamma_\Lambda^{\bar{c}_\uparrow \bar{c}_\downarrow \psi} = \Gamma_\Lambda^{c_\downarrow c_\uparrow \bar{\psi}} \approx 1, \quad (4.25)$$

see Eq. (3.6). In Appendix E we shall use a more elaborate truncation strategy where the RG flow of the three-point vertices $\Gamma_\Lambda^{\bar{c}_\uparrow \bar{c}_\downarrow \psi}$, $\Gamma_\Lambda^{c_\downarrow c_\uparrow \bar{\psi}}$ and the mixed four-point vertex $\Gamma_\Lambda^{\bar{c}_\sigma c_\sigma \bar{\psi} \psi}$ is regained. However, our main result for the quasiparticle damping derived in this subsection is not qualitatively modified by the higher order vertex corrections represented by the RG flow of $\Gamma_\Lambda^{\bar{c}_\uparrow \bar{c}_\downarrow \psi}$, $\Gamma_\Lambda^{c_\downarrow c_\uparrow \bar{\psi}}$, and $\Gamma_\Lambda^{\bar{c}_\sigma c_\sigma \bar{\psi} \psi}$.

Since we are interested in the effect of classical critical fluctuations, we retain only the contribution from the zeroth Matsubara frequency to the right-hand side of the flow equation (3.12). After analytic continuation to the real frequencies we obtain the following FRG flow equation for the fermionic self-energy,

$$\begin{aligned} \partial_\Lambda \Sigma_\Lambda(\mathbf{k}, \omega + i0^+) = \\ T \int_{\mathbf{p}} \frac{\dot{F}_\Lambda(\mathbf{p})}{\omega + \xi_{\mathbf{p}-\mathbf{k}} + \Sigma_\Lambda(\mathbf{p} - \mathbf{k}, -\omega - i0^+)}. \end{aligned} \quad (4.26)$$

We approximate the flowing static single-scale propagator by its long wavelength limit

$$\dot{F}_\Lambda(\mathbf{p}) \approx \frac{-\delta(p - \Lambda)}{r_\Lambda + c_\Lambda \Lambda^2}. \quad (4.27)$$

The parameters r_Λ and c_Λ are determined by the FRG flow equation (3.13) for the bosonic self-energy $\Phi_\Lambda(P)$ shown graphically in Fig. 7 (b). Since we are only interested in classical fluctuations we may set all Matsubara frequencies equal to zero in these equations and obtain

$$\partial_\Lambda r_\Lambda = T \int_{\mathbf{p}} \dot{F}_\Lambda(\mathbf{p}) \Gamma_\Lambda^{\bar{\psi} \bar{\psi} \psi \psi}(0, \mathbf{p}; \mathbf{p}, 0), \quad (4.28)$$

$$\partial_\Lambda c_\Lambda = T \int_{\mathbf{p}} \dot{F}_\Lambda(\mathbf{p}) \lim_{q \rightarrow 0} \frac{\partial}{\partial q^2} \Gamma_\Lambda^{\bar{\psi} \bar{\psi} \psi \psi}(\mathbf{q}, \mathbf{p}; \mathbf{p}, \mathbf{q}). \quad (4.29)$$

Note that the parameter c_Λ is related to the scale-dependent anomalous dimension η_Λ of the superfluid order parameter field as follows¹⁷

$$\eta_\Lambda = \Lambda \partial_\Lambda \ln \left(\frac{c_0}{c_\Lambda} \right) = -\frac{\Lambda \partial_\Lambda c_\Lambda}{c_\Lambda}. \quad (4.30)$$

Our truncated FRG flow equation (4.26) therefore contains both the effect of the anomalous dimension of the superfluid order parameter and the damping of intermediate states. In fact, our evaluation of the self-energy in Gaussian approximation presented in Sec. IV A shows that critical fluctuations mainly renormalize the imaginary part of the self-energy. We therefore ignore the real part of the self-energy in Eq. (4.26) and focus on the FRG flow of its imaginary part on the Fermi surface,

$$\gamma_\Lambda = -\text{Im} \Sigma_\Lambda(\mathbf{k}_F, i0^+). \quad (4.31)$$

This quasiparticle damping is determined by the flow equation

$$\partial_\Lambda \gamma_\Lambda = -T \int_{\mathbf{p}} \frac{\delta(p - \Lambda)}{r_\Lambda + c_\Lambda \Lambda^2} \frac{\gamma_\Lambda}{\gamma_\Lambda^2 + \xi_{\mathbf{p}-\mathbf{k}_F}^2}. \quad (4.32)$$

Assuming $\Lambda \ll k_F$ we may linearize the energy dispersion around the Fermi surface, $\xi_{\mathbf{p}-\mathbf{k}_F} \approx -\mathbf{v}_F \cdot \mathbf{p}$. In three dimensions, the angular integration is then elementary and we obtain for the flow of the quasiparticle damping on the Fermi surface,

$$\partial_\Lambda \gamma_\Lambda = -K_3 \frac{T \Lambda \arctan(v_F \Lambda / \gamma_\Lambda)}{v_F r_\Lambda + c_\Lambda \Lambda^2}, \quad (4.33)$$

where

$$K_3 = 1/(2\pi^2). \quad (4.34)$$

To obtain the self-consistent quasiparticle damping from Eq. (4.33), we need additional RG flow equations for the two parameters r_Λ and c_Λ . Within our classical approximation this flow is determined by Eqs. (4.28) and (4.29) which depend on the induced interaction $\Gamma_\Lambda^{\bar{\psi} \bar{\psi} \psi \psi}(\mathbf{p}'_1, \mathbf{p}'_2; \mathbf{p}_2, \mathbf{p}_1)$ between classical order parameter fluctuations. Note that in our interaction-momentum cutoff scheme the FRG flow of all vertices without fermionic external legs is completely decoupled from the FRG flow of the other vertices with fermionic legs so that we may use the strategy developed in Refs. [46 and 47] to obtain a closed systems of RG flow equations for r_Λ and c_Λ . In a first step, we define

$$u_\Lambda = \Gamma_\Lambda^{\bar{\psi} \bar{\psi} \psi \psi}(0, 0; 0, 0), \quad (4.35)$$

and neglect the momentum-dependence of $\Gamma_\Lambda^{\bar{\psi} \bar{\psi} \psi \psi}(\mathbf{q}, \mathbf{p}; \mathbf{p}, \mathbf{q})$ on the right-hand sides of the flow equations (4.28) and (4.29). In this approximation c_Λ does not flow and the RG flow of r_Λ is

$$\partial_\Lambda r_\Lambda = -K_3 T \frac{u_\Lambda \Lambda^2}{r_\Lambda + c_\Lambda \Lambda^2}. \quad (4.36)$$

To obtain the RG flow of the interaction u_Λ , we neglect again the momentum-dependence of the four-point vertices on the right-hand side of the flow equation (3.17) for the induced interaction between order parameter fluctuations and obtain

$$\partial_\Lambda u_\Lambda = \frac{5}{2} K_3 T \frac{u_\Lambda^2 \Lambda^2}{[r_\Lambda + c_\Lambda \Lambda^2]^2}, \quad (4.37)$$

where we have also neglected the flow of the six-point vertex. Actually, as discussed in Sec. III, within our cutoff scheme the GM correction to the critical temperature can be obtained by calculating the effect of the initial value of the six-point vertex on the bosonic self-energy to second order in the Gaussian propagator of the order parameter field, see Fig. 6 (c). In our FRG approach this contribution can be simply taken into account via the initial condition $r_0 \propto T - T_c$, where the value of T_c includes the GM correction. Finally, to obtain the RG of c_Λ and the associated flowing anomalous dimension η_Λ from Eq. (4.30), we need the momentum-dependence of the induced interaction $\Gamma_\Lambda^{\bar{\psi}\bar{\psi}\psi\psi}(\mathbf{p}'_1, \mathbf{p}'_2; \mathbf{p}_2, \mathbf{p}_1)$, which is determined by the exact FRG flow equation (3.17) shown graphically in Fig. 9. Following Refs. 46 and 47, we obtain an approximate solution of this flow equation by neglecting the flowing six-point vertex as well as the momentum-dependence of the four-point vertices on the right-hand side. Moreover, since we are interested in classical order parameter fluctuations, we only need the classical component of the interaction which can be obtained by setting all external Matsubara frequencies in our exact flow equation (3.17) equal to zero. With these approximations we obtain for the momentum-dependent induced interaction between order parameter fluctuations,

$$\begin{aligned} \partial_\Lambda \Gamma_\Lambda^{\bar{\psi}\bar{\psi}\psi\psi}(\mathbf{p}'_1, \mathbf{p}'_2; \mathbf{p}_2, \mathbf{p}_1) &\approx -u_\Lambda^2 \left[\frac{1}{2} I_\Lambda(\mathbf{p}_1 + \mathbf{p}_2) \right. \\ &\quad \left. + I_\Lambda(\mathbf{p}_1 - \mathbf{p}'_1) + I_\Lambda(\mathbf{p}_2 - \mathbf{p}'_1) \right], \end{aligned} \quad (4.38)$$

where

$$I_\Lambda(\mathbf{p}) = 2T \int_{\mathbf{q}} \dot{F}_\Lambda(\mathbf{q}) F_\Lambda(\mathbf{q} + \mathbf{p}). \quad (4.39)$$

Integrating Eq. (4.38) over the flow parameter Λ we find for the induced two-body interaction between classical superfluid fluctuations

$$\begin{aligned} \Gamma_\Lambda^{\bar{\psi}\bar{\psi}\psi\psi}(\mathbf{p}'_1, \mathbf{p}'_2; \mathbf{p}_2, \mathbf{p}_1) &= \Gamma_{\Lambda_0}^{\bar{\psi}\bar{\psi}\psi\psi}(\mathbf{p}'_1, \mathbf{p}'_2; \mathbf{p}_2, \mathbf{p}_1) \\ &\quad + \int_{\Lambda}^{\Lambda_0} d\Lambda' u_{\Lambda'}^2 \left[\frac{1}{2} I_{\Lambda'}(\mathbf{p}_1 + \mathbf{p}_2) \right. \\ &\quad \left. + I_{\Lambda'}(\mathbf{p}_1 - \mathbf{p}'_1) + I_{\Lambda'}(\mathbf{p}_2 - \mathbf{p}'_1) \right]. \end{aligned} \quad (4.40)$$

Recall that in our cutoff scheme the initial value $\Gamma_{\Lambda_0}^{\bar{\psi}\bar{\psi}\psi\psi}(\mathbf{p}'_1, \mathbf{p}'_2; \mathbf{p}_2, \mathbf{p}_1)$ of the induced interaction is given by the symmetrized closed fermion loop defined in Eq. (3.8) (see also Fig. 6 (a)), which is momentum-dependent. Substituting Eq. (4.40) into our flow equation (4.29) for the coupling c_Λ we find for the flowing

anomalous dimension defined in Eq. (4.30),

$$\begin{aligned} \eta_\Lambda &= -\frac{\Lambda T}{c_\Lambda} \int_{\mathbf{p}} \dot{F}_\Lambda(\mathbf{p}) \lim_{\mathbf{q} \rightarrow 0} \frac{\partial}{\partial q^2} \Gamma_{\Lambda_0}^{\bar{\psi}\bar{\psi}\psi\psi}(\mathbf{q}, \mathbf{p}; \mathbf{p}, \mathbf{q}) \\ &\quad - \frac{3}{2} \frac{\Lambda T}{c_\Lambda} \int_{\mathbf{p}} \dot{F}_\Lambda(\mathbf{p}) \int_{\Lambda}^{\Lambda_0} d\Lambda' u_{\Lambda'}^2 \lim_{\mathbf{q} \rightarrow 0} \frac{\partial}{\partial q^2} I_{\Lambda'}(\mathbf{p} + \mathbf{q}). \end{aligned} \quad (4.41)$$

From the explicit expression for the initial interaction $\Gamma_{\Lambda_0}^{\bar{\psi}\bar{\psi}\psi\psi}(\mathbf{p}'_1, \mathbf{p}'_2; \mathbf{p}_2, \mathbf{p}_1)$ in Eq. (3.8) we obtain for $p \lesssim p_0$ the estimate

$$\begin{aligned} &\lim_{\mathbf{q} \rightarrow 0} \frac{\partial}{\partial q^2} \Gamma_{\Lambda_0}^{\bar{\psi}\bar{\psi}\psi\psi}(\mathbf{q}, \mathbf{p}; \mathbf{p}, \mathbf{q}) \\ &\approx \lim_{\mathbf{q} \rightarrow 0} \frac{\partial}{\partial q^2} \Gamma_{\Lambda_0}^{\bar{\psi}\bar{\psi}\psi\psi}(\mathbf{q}, 0; 0, \mathbf{q}) = -A_0 u_0 / p_0^2, \end{aligned} \quad (4.42)$$

where A_0 is a numerical constant of the order of unity and $u_0 = \Gamma_{\Lambda_0}^{\bar{\psi}\bar{\psi}\psi\psi}(0, 0; 0, 0)$ is given in Eq. (3.9). It is then easy to see that the first term in Eq. (4.41) cannot modify the fixed point limit of η_Λ for $\Lambda \rightarrow 0$, so that from now on we shall omit this term. The resulting system of coupled RG flow equations for the three couplings r_Λ , c_Λ and u_Λ is then formally identical to the system discussed in Refs. 46 and 47. Introducing the logarithmic flow parameter $l = \ln(\Lambda_0/\Lambda)$, the RG flow of the dimensionless rescaled couplings

$$\tilde{r}_l = \frac{r_\Lambda}{c_\Lambda \Lambda^2}, \quad (4.43)$$

$$\tilde{u}_l = \frac{K_3 T u_\Lambda}{c_\Lambda^2 \Lambda} \quad (4.44)$$

is given by

$$\partial_l \tilde{r}_l = (2 - \eta_l) \tilde{r}_l + \frac{\tilde{u}_l}{1 + \tilde{r}_l}, \quad (4.45)$$

$$\partial_l \tilde{u}_l = (1 - 2\eta_l) \tilde{u}_l - \frac{5}{2} \frac{\tilde{u}_l^2}{(1 + \tilde{r}_l)^2}. \quad (4.46)$$

The scale-dependent anomalous dimension satisfies the integral equation

$$\eta_l = \int_0^l dt K(l, t) u_{l-t}^2 e^{-2 \int_{l-t}^l d\tau \eta_\tau}, \quad (4.47)$$

where the kernel $K(l, t)$ can be expressed in terms of the dimensionless function

$$f_l(p/\Lambda) = -\frac{\Lambda^2 c_\Lambda^2}{K_3 T} I_\Lambda(\mathbf{p}) \quad (4.48)$$

as follows,

$$K(l, t) = \frac{1}{4(1 + \tilde{r}_l)} [2f'_{l-t}(e^{-t}) + e^{-t} f''_{l-1}(e^{-t})]. \quad (4.49)$$

Here $f'_l(x)$ and $f''_l(x)$ denote the first and the second derivative of $f_l(x)$.

At the critical temperature the rescaled couplings \tilde{r}_l , \tilde{u}_l , and η_l approach finite limits for $l \rightarrow \infty$. In Fig. 13

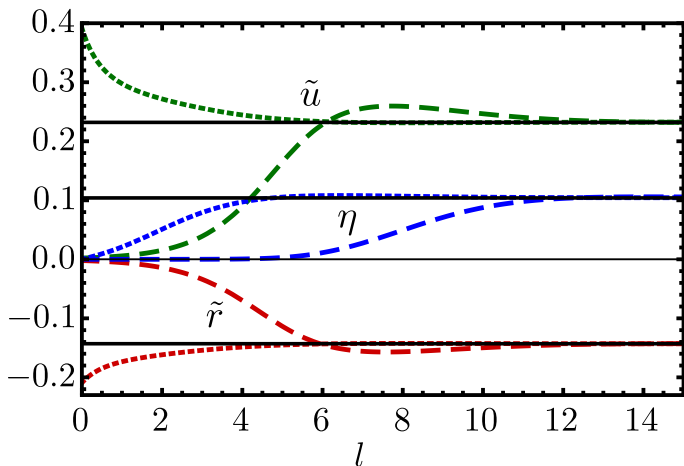


FIG. 13. RG flow of the flowing anomalous dimension η_l and dimensionless couplings \tilde{r}_l and \tilde{u}_l obtained from the numerical solution of the coupled integro-differential equations (4.45–4.47) for two different critical temperatures: $T = T_c = 0.13E_F$ (dotted lines), $T = T_c = 0.01E_F$ (dashed lines). The black solid lines mark the fixed point values given in Eqs. (4.50a–4.50c).

we plot the flow of \tilde{r}_l , \tilde{u}_l , and η_l for two different values of the critical temperature as an example. Within our simple truncation the fixed point values are^{46,47}

$$\tilde{r}_* = -0.143, \quad (4.50a)$$

$$\tilde{u}_* = 0.232, \quad (4.50b)$$

$$\eta_* = 0.104. \quad (4.50c)$$

Note that the fixed point value of the anomalous dimension η_* is larger than the accepted value $\eta = 0.038$ for the XY-universality class in three dimensions,⁴⁵ this discrepancy can be significantly reduced using more sophisticated truncation strategies^{47,48} of the FRG flow equations. For our purpose, the simple truncation strategy described above is sufficient.

Given the RG flow of the rescaled quantities \tilde{r}_l , \tilde{u}_l , and η_l , we can reconstruct the flow of the dimensionful relevant coupling $r_\Lambda = c_\Lambda \Lambda^2 \tilde{r}_l$ and of the marginal coupling

$$c_\Lambda = c_0 \exp \left[\int_0^{\ln(\Lambda_0/\Lambda)} dt \eta_t \right], \quad (4.51)$$

which we need for calculating the quasiparticle damping γ_Λ from the flow equation (4.33).

By solving the coupled flow equations (4.45), (4.46), and (4.47) for various temperatures and using the result as an input for the flow equation (4.33) for the quasiparticle damping we obtain the quasiparticle damping $\gamma(T)$ as a function of the temperature. Our numerical result for the damping $\gamma(T_c)$ as a function of the critical temperature T_c is plotted in Fig. 14. In the weak coupling regime $T_c \ll E_F$ the quasiparticle damping due to classical critical fluctuations is described by the interpolation

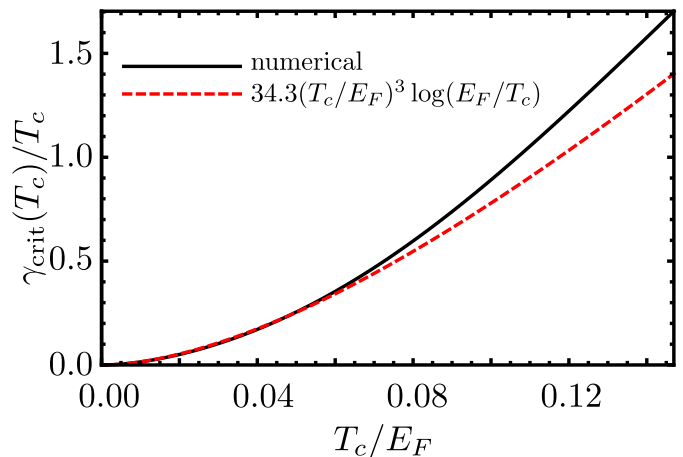


FIG. 14. Quasiparticle damping $\gamma(T_c)$ as a function of the critical temperature T_c . The black solid line represents the numerical solution of the FRG flow equations (4.45), (4.46), (4.47) and (4.33). The red dashed line is a fit to the interpolation formula (4.52) with $C = 34.3$.

formula

$$\gamma_{\text{crit}}(T_c) \approx C \frac{T_c^3}{E_F^2} \ln \left(\frac{E_F}{T_c} \right), \quad (4.52)$$

where the numerical value of the prefactor is

$$C \approx 34.3. \quad (4.53)$$

Using Eq. (4.6) to express the the logarithm $\ln(E_F/T_c)$ in Eq. (4.52) in terms of the Ginzburg-Levanyuk number Gi we can express the quasiparticle damping due to critical fluctuations in the form (1.2) given in the introduction.

The appearance of the logarithm in Eq. (4.52) is related to the logarithmic divergence of the quasi-particle damping encountered in Gaussian approximation, see Eq. (4.16). Note that the numerical value of the prefactor C is rather large. Although the precise numerical value of C given above is an artifact of our truncation scheme, we show in Appendix E that a more sophisticated truncation including the RG flow of the three-point and mixed four-point vertices confirms the validity of Eq. (4.52) with a prefactor $C \approx 18$ which is still large compared with unity.

The above results should be compared with the well known quadratic low-temperature behavior of the quasiparticle damping in a three-dimensional Fermi liquid, see Eq. (4.18). At $T = T_c$ the Fermi liquid damping is

$$\gamma_{\text{FL}}(T_c) = C_{\text{FL}} T_c^2 / E_F, \quad (4.54)$$

where the numerical value of C_{FL} depends on the strength of the screened interaction but is usually close to unity.⁴² Although for sufficiently small T_c the Fermi liquid damping is always larger than the damping due to critical superconducting fluctuations discussed above, due to the large prefactor in Eq. (4.52) there is a substantial temperature regime where the damping due to critical fluctuations dominates. Note also that short-range

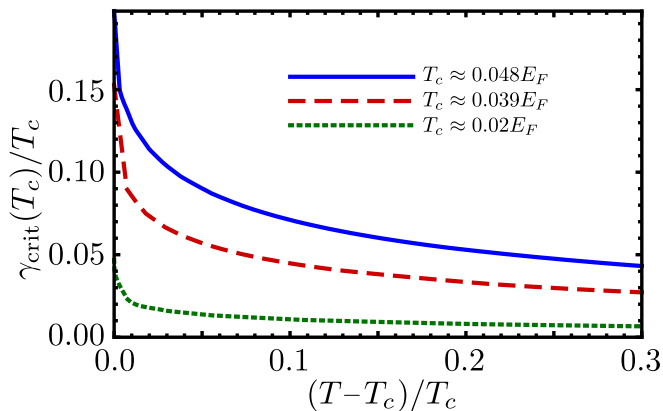


FIG. 15. FRG result for the temperature dependence of the quasiparticle damping $\gamma(T)$ as a function of t for different values of T_c .

interactions in Fermi liquids give rise to a non-analytic correction of the form (4.52), see Ref. [44]. However, the corresponding prefactor C_{FL} is of order unity, so that the numerical value of the prefactor of the non-analytic $T^3 \ln T$ -contribution to the quasi-particle damping at T_c is dominated by classical critical fluctuations. Moreover, for $T > T_c$ the quasi-particle damping $\gamma(T)$ due to classical critical fluctuations is a decreasing function of temperature, as shown in Fig. 15. This is very different from any perturbative correction to the quasi-particle damping, which usually increases with temperature. The fact that the contribution from classical critical fluctuations to $\gamma(T)$ grows as the temperature is lowered is closely related to the logarithmic divergence of the damping for $T \rightarrow T_c$ encountered within the Gaussian approximation, see Eq. (4.16). Note that, in contrast to the result for the Gaussian approximation, our FRG result for the damping approaches a finite limit for $T \rightarrow T_c$, as given in Eqs. (4.52). The decrease of relaxation rates with temperature as one moves away from the critical point has also been observed for disordered metals above the superconducting transition.¹ In Fig. 16 we illustrate the regime in the plane spanned by the interaction length (which we parametrize by T_c) and the temperature where the damping $\gamma(T)$ due to classical pairing fluctuations obtained from our FRG approach is larger than the Fermi liquid damping $\gamma_{\text{FL}}(T) \approx T^2/E_F$, see Eq. (4.18). Obviously, the colorful area where this condition is fulfilled is sizable even for rather small values of the interaction.

Finally, let us point out that our result (4.52) for the quasiparticle damping due to classical critical fluctuations is not qualitatively modified by vertex corrections. In Appendix E we present an improved truncation of the FRG flow equations where we retain, in addition to the purely bosonic vertices in Eqs. (4.45-4.47) and the fermionic self-energy in Eq. (4.33), the three-legged vertices $\Gamma_{\Lambda}^{\bar{c}_{\uparrow} \bar{c}_{\downarrow} \psi}$, $\Gamma_{\Lambda}^{c_{\downarrow} c_{\uparrow} \bar{\psi}}$, as well as the mixed four-legged vertex $\Gamma_{\Lambda}^{\bar{c}_{\sigma} c_{\sigma} \bar{\psi} \psi}$. From the numerical solution of the extended

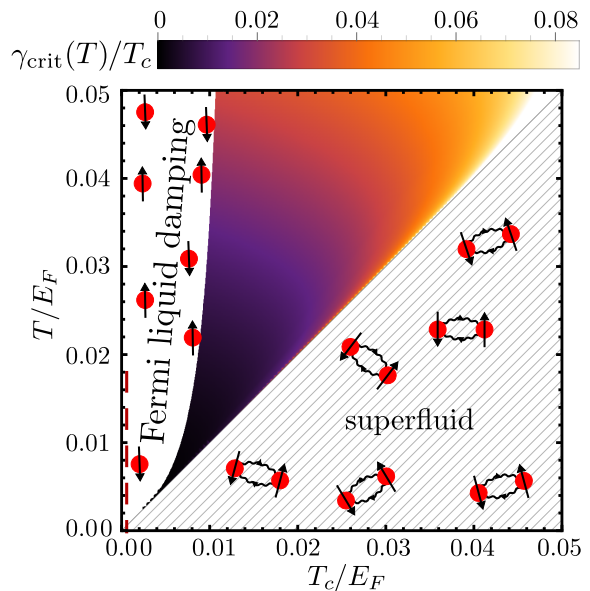


FIG. 16. The colorful area represents the regime in the plane spanned by the interaction length (parametrized by the dimensionless parameter T_c/E_F) and temperature where the quasi-particle damping due to classical pairing fluctuations $\gamma(T)$ obtained from our FRG approach is larger than the Fermi liquid result $\gamma_{\text{FL}} \approx T^2/E_F$. In the white region γ_{FL} is still larger than $\gamma_{\text{crit}}(T)$.

set of the flow equations we can confirm the validity of Eq. (4.52) with a modified prefactor $C \approx 18$, which is still large compared with unity.

V. SUMMARY AND CONCLUSIONS

In this work we have used functional renormalization group methods to study the effect of static pairing fluctuations on the electronic properties of metals in the critical (Ginzburg) region above the superconducting transition temperature. Our approach is based on partial bosonization of the electron-electron interaction in the particle-particle channel and the application of FRG methods to the resulting mixed Bose-Fermi model within a special cutoff scheme where a regulator is introduced only in the bosonic sector (interaction-momentum cutoff scheme). To illustrate the efficiency of our approach, we have re-derived in a simplified way the correction to T_c obtained by Gorkov and Melik-Barkhudarov¹⁰ by identifying T_c with the temperature where the gap of the inverse bosonic propagator vanishes. Moreover, we have shown, within our more streamlined approach, that this correction to T_c is changed by a numerical factor when the chemical potential is fixed instead of the particle density. Another advantage of our approach is that it allows us to understand the emergence of various types of induced interaction vertices involving pairing fluctuations from the renormalization group point of view.

We have then used our powerful method to study the

effect of critical pairing fluctuations on the electronic single-particle excitations in the normal state, especially on the electronic density of states and on the damping γ of quasiparticles with momenta on the Fermi surface. Within the Gaussian approximation (which corresponds to the ladder or T -matrix approximation for the effective two-body interaction) we have found an (up to now unnoticed) logarithmic divergence of the quasiparticle damping $\gamma \propto T_c^3 \ln[T_c/(T - T_c)]$ for $T \rightarrow T_c$, while the density of states exhibits a finite pseudogap. At this level of approximation a finite value of γ can only be introduced by invoking other interaction processes, for instance inelastic electron-electron collisions within Fermi liquid theory⁴² that are further enhanced by disorder present in real materials due to the weak localization effect.^{49–51} The logarithmic divergence of γ encountered in Gaussian approximation implies that Gaussian pairing fluctuations completely destroy the Fermi liquid behavior of the single-particle Green function at and slightly above the critical temperature. In view of the fact that in three dimensions the critical fluctuations of the pairing field are not controlled by the Gaussian fixed point this is perhaps not so surprising. Note also that for $T < T_c$, i.e. in the superfluid phase, order parameter fluctuations are known to have a strong effect on the single-particle properties. For example, in Ref. 9 it has been shown that at $T = 0$ Gaussian fluctuations of the pairing field give rise to a logarithmic suppression of the quasiparticle residue and the density of states.

Given the fact the Gaussian approximation is not sufficient, we have used the FRG to take the non-Gaussian nature of critical pairing fluctuations into account, which is the main technical part of our work. Let us point out that this approach should also be useful for a systematic evaluation of corrections to the Gaussian approximation in other cases where the dominant scattering channel between electrons can be uniquely identified on physical grounds. It is then convenient to treat the dominant channel non-perturbatively using a suitable Hubbard-Stratonovich field, so that the Gaussian approximation for this field amounts to solving a single-channel Bethe-Salpeter equation for the effective interaction. Other scattering channels and the corresponding vertex corrections can then be taken into account approximately via the induced interaction vertices which are generated as we integrate the FRG flow equations. A similar strategy is adopted by the dynamical re-bosonization method,³² which is, however, restricted to situations where the momentum- and frequency dependence of the induced interactions can be neglected.

In the fluctuation regime just above T_c our FRG approach gives a finite relaxation rate of the fermionic quasiparticles, which increases down to the transition temperature but remains finite at the transition point, $\gamma_{\text{crit}} = CT_c^3/E_F^2 \log(E_F/T_c)$, where the numerical constant C is large compared with unity. Physically, the corresponding finite lifetime $\tau_{\text{crit}} = 1/\gamma_{\text{crit}}$ of quasiparticles on the Fermi surface is due to collisions between the un-

paired fermions and virtually formed Cooper pairs associated with critical pairing fluctuations. This is similar to the effect of a disorder potential on the phase coherence of quasi-particles in dirty systems,^{52–54} where limited applicability of the ergodicity hypothesis makes direct observation of some of the coherence effects harder.^{55,56}

It is tempting to associate τ_{crit} with the phase breaking time τ_φ due to the Anderson's theorem,⁵⁷ which is applicable to the s-type superconductor studied in the present work. However, its manifestation in the particle-particle (fluctuation) propagator has only been studied within the ladder approximation, see Ref. [58] and a comprehensive book by Larkin and Varlamov.¹ The finite quasi-particle lifetime obtained in Eq. (4.52) requires essentially a beyond ladder approach, i.e. renormalization of the bosonic line in the second term in Fig. 7(a) corresponds to a sum over the ladder diagrams in Eq. (4.1) but renormalization of the fermionic line accounts for more diagrams of a different type; here we refer to the analysis in Subsec. IIIB where the first term in Fig. 7(a) is neglected. Thus, the two-particle correlation function would need to be calculated using the approach developed in this paper in order to put such an interpretation on a solid ground, which could be a subject of a future work.

At higher temperatures above T_c the Fermi liquid damping^{42,43} $\gamma_{\text{FL}} \simeq T^2/E_F$ becomes larger, but close to the transition temperature there is a finite region where the damping in clean systems is dominated by critical fluctuations, as shown in Fig. 16. To be specific, we estimate that the effect of critical pairing fluctuations can be seen if the critical temperature is larger than $T_c^* \approx 2 \times 10^{-4} E_F$. With $E_F = 2$ eV this gives $T_c^* \approx 5$ K, so that the contribution of critical pairing fluctuations to the quasiparticle damping should be observable in superconductors with $T_c \gtrsim 5$ K.

Our approach also provides a microscopic and fully consistent theory for the pseudogap in a clean electronic system originating from the superconducting fluctuations only. The density of states in Eq. (4.8) evaluated using the result of the FRG in Eq. (4.31) is significantly different from the Gaussian approximation in Eq. (4.7). The former result predicts a partial suppression of the density of states at the Fermi energy and a finite quasi-particle relaxation rate down to the point of the superconducting transition. Fitting the result of our numerical integration of the FRG equations in subsection V, we find for the leading order behavior for the density of states at the Fermi level in the weak coupling regime,

$$\frac{\nu_0 - \nu}{\nu_0} \propto \left(\frac{T_c}{E_F} \right)^2 \propto \sqrt{Gi}. \quad (5.1)$$

This functional dependence of the pseudogap strength on T_c should be observable in clean superconductors with higher T_c , which transition temperatures exceeding our estimate for T_c^* given above.

Generally, the effect of critical pairing fluctuations on the electronic spectrum is most pronounced in strongly coupled superconductors with small coherence length and

broad fluctuation regimes, corresponding to Ginzburg-Levanyuk numbers Gi of the order of unity. For instance, this regime should be relevant for the normal state of the cuprate superconductors,^{59–64} which exhibits a pseudogap and a linear temperature dependence of the quasiparticle damping, in agreement with our prediction. Another class of fermionic superfluids where fluctuation effects T_c can be studied experimentally are ultracold gases of fermionic atoms or molecules. In these systems the effective two-body interaction can be controlled using the Feshbach-resonance technique.⁴ In particular, in the vicinity of the unitary point where the scattering length diverges, fluctuation effects above T_c are expected to be most pronounced. It should be interesting to extend the calculations for the quasi-particle damping and the pseudogap presented in this work to the unitary point and discuss the BCS-BEC crossover of these quantities.

ACKNOWLEDGEMENTS

We thank Andrey Varlamov for many useful discussions and for his insightful suggestions and comments on the manuscript. We also thank Casper Druker for his contributions at initial states of this work and acknowledge financial support by the DFG through SFB/TRR 49 and FOR 723.

APPENDIX A: INTERACTION CORRECTIONS TO THE PARTICLE-PARTICLE BUBBLE

The self-energy $\Phi(P)$ of the pairing field introduced in Eq. (2.6) can be identified with the renormalized particle-particle bubble. In this appendix we will explicitly evaluate the regularized non-interacting bubble $\Phi_0^{\text{reg}}(0)$ defined in Eq. (2.19) and the first two interaction corrections $\Phi_1(0)$ and $\Phi_2(0)$ given in Eqs. (2.25) and (2.26) for vanishing total momentum and energy.

Consider first the non-interacting particle-particle bubble $\Phi_0(P)$ defined in Eq. (2.7). After performing the Matsubara sum and setting $P = (\mathbf{p}, i\bar{\omega})$ we obtain

$$\begin{aligned} \Phi_0(\mathbf{p}, i\bar{\omega}) &= \int_K G_0(K)G_0(P-K) \\ &= \int_{\mathbf{k}} \Theta(\Lambda_0 - |\mathbf{k}|) \frac{1 - f(\xi_{\mathbf{k}}) - f(\xi_{\mathbf{p}-\mathbf{k}})}{\xi_{\mathbf{k}} + \xi_{\mathbf{p}-\mathbf{k}} - i\bar{\omega}} \\ &= \int_{\mathbf{k}} \Theta(\Lambda_0 - |\mathbf{k}|) \frac{\tanh(\beta\xi_{\mathbf{k}}/2)}{\xi_{\mathbf{k}} + \xi_{\mathbf{p}-\mathbf{k}} - i\bar{\omega}}, \end{aligned} \quad (\text{A1})$$

where $\xi_{\mathbf{k}} = \epsilon_{\mathbf{k}} - \mu$, $f(\xi_{\mathbf{k}}) = 1/(e^{\beta\xi_{\mathbf{k}}} + 1)$ is the Fermi function, and we have defined the integration symbol $\int_{\mathbf{k}} = \int \frac{d^3k}{(2\pi)^3}$. The ultraviolet cutoff $\Lambda_0 \gg k_F$ restricts the momentum integration to the regime $|\mathbf{k}| \leq \Lambda_0$. We assume that the external momentum satisfies $\Lambda_0 \gg |\mathbf{p}|$ so that the shift in the integration variable in the third line of Eq. (A1) does not affect the cutoff. At $P = 0$ the

integral in the last line of Eq. (A1) can be transformed to a dimensionless form by substituting $x = \epsilon_{\mathbf{k}}/E_F$,

$$\Phi_0(0) = \nu \int_0^{\lambda_0^2} dx \sqrt{x} \frac{\tanh\left(\frac{x-\mu/E_F}{2\tau}\right)}{2(x-\mu/E_F)}, \quad (\text{A2})$$

where $\lambda_0 = \Lambda_0/k_F$, $\tau = T/E_F$, and $\nu = mk_F/(2\pi^2)$ is the density of states at the Fermi energy per spin projection. We focus on the BCS regime where $\mu \approx E_F$. The asymptotic behavior of this integral for $\tau \ll 1$ can then be extracted following the procedure outlined by GM¹⁰ and we finally obtain

$$\Phi_0(0) = \nu [\ln(A/\tau) + \lambda_0 + \mathcal{O}(\tau, \lambda_0^{-1})], \quad (\text{A3})$$

with the numerical constant $A = 8/(\pi e^{2-\gamma_E})$, see Eq. (2.29). If we subtract from $\Phi_0(P)$ the vacuum bubble defined in Eq. (2.16) the cutoff-dependent term $\nu\lambda_0$ on the right-hand side of (A3) is canceled so that we may take the limit $\lambda_0 \rightarrow \infty$ and obtain the low-temperature asymptotics of the regularized particle-particle bubble given in Eq. (2.28).

Next, let us evaluate the second order correction $\Phi_2(0)$ to the particle-particle bubble arising from the induced interaction in the particle-hole channel, which according to Eq. (2.26) can be written as

$$\begin{aligned} \Phi_2(0) &\approx g^2 \int_K \int_{K'} G_0(K)G_0(-K) \\ &\quad \times \Pi_0(K-K')G_0(K')G_0(-K'), \end{aligned} \quad (\text{A4})$$

where the non-interacting particle-hole bubble $\Pi_0(Q)$ is defined in Eq. (2.23). It turns out that this integral is still ultraviolet divergent so that we introduce again an ultraviolet cutoff $\Lambda_0 \gg k_F$ as in Eq. (A1). Following GM, we simplify the integrand in Eq. (A4) as follows:

1. Neglect the frequency dependence of the particle hole bubble,

$$\Pi_0(K-K') \approx \Pi_0(\mathbf{k}-\mathbf{k}', 0). \quad (\text{A5})$$

2. Project the momentum dependence of the particle-hole bubble onto the Fermi surface,

$$\Pi_0(\mathbf{k}-\mathbf{k}', 0) \approx \Pi_0(\mathbf{k}_F - \mathbf{k}'_F, 0), \quad (\text{A6})$$

where \mathbf{k}_F is the point on the Fermi surface closest to \mathbf{k} .

By numerically evaluating Eq. (A4) we have explicitly verified that the above approximations do not modify the prefactor of the leading $\ln^2(1/\tau)$ dependence of $\Phi_2(0)$ given in Eq. (2.34), which determines the fluctuation correction to T_c in the weak coupling limit. With these approximations the second order correction (A4) to the particle-particle bubble reduces to

$$\Phi_2(0) \approx g^2 \int_K \int_{K'} G_0(K)G_0(-K)\Pi_0(\mathbf{k}_F - \mathbf{k}'_F, 0)$$

$$\times G_0(K')G_0(-K'). \quad (\text{A7})$$

The particle-hole bubble is given by

$$\begin{aligned} \Pi_0(Q) &= \int_K G_0(K)G_0(K-Q) \\ &= \int \frac{d^3k}{(2\pi)^3} \frac{f(\xi_{\mathbf{k}}) - f(\xi_{\mathbf{k}-\mathbf{q}})}{\xi_{\mathbf{k}} - \xi_{\mathbf{k}-\mathbf{q}} - i\bar{\omega}}. \end{aligned} \quad (\text{A8})$$

At zero temperature and in the static limit ($\bar{\omega} = 0$) this reduces to

$$\Pi_0(\mathbf{q}, 0) = -\nu \left[\frac{1}{2} + \frac{1 - \tilde{q}^2}{4\tilde{q}} \ln \left| \frac{1 + \tilde{q}}{1 - \tilde{q}} \right| \right], \quad (\text{A9})$$

where $\tilde{q} = |\mathbf{q}|/(2k_F)$ and ν is the density of states at the Fermi energy. Setting

$$|\mathbf{k}_F - \mathbf{k}'_F| = k_F \sqrt{2 - 2 \cos \vartheta}, \quad (\text{A10})$$

where ϑ is the angle between \mathbf{k}_F and \mathbf{k}'_F , we may expand $\Pi_0(\mathbf{k}_F - \mathbf{k}'_F, 0)$ in Legendre polynomials $P_l(\cos \vartheta)$,

$$\Pi_0(\mathbf{k}_F - \mathbf{k}'_F, 0) = \sum_{l=0}^{\infty} a_l P_l(\cos \vartheta), \quad (\text{A11})$$

where

$$a_l = \frac{2l+1}{2} \int_{-1}^1 dx \Pi_0(k_F \sqrt{2-2x}, 0) P_l(x). \quad (\text{A12})$$

Actually, the integration in Eq. (A7) projects out the $l=0$ component so that under the integral sign we may replace $\Pi_0(\mathbf{k}_F - \mathbf{k}'_F, 0)$ by its angular average

$$\begin{aligned} a_0 &= \frac{1}{2} \int_{-1}^1 dx \Pi_0(k_F \sqrt{2-2x}, 0) \\ &= -\nu \int_0^1 dy \left[\frac{1}{2} + \frac{1-y}{4\sqrt{y}} \ln \left| \frac{1+\sqrt{y}}{1-\sqrt{y}} \right| \right] = \nu \alpha_2, \end{aligned} \quad (\text{A13})$$

where the numerical constant $\alpha_2 < 0$ is given in Eq. (2.35). The second order correction to the particle-particle bubble then reduces to

$$\begin{aligned} \Phi_2(0) &= g^2 a_0 \left[\int_K G_0(K)G_0(-K) \right]^2 = g^2 \nu \alpha_2 [\Phi_0(0)]^2 \\ &= g^2 \nu^3 \alpha_2 [\ln(A/\tau) + \lambda_0]^2, \end{aligned} \quad (\text{A14})$$

as given in Eq. (2.34) of the main text. The cutoff-dependence in Eq. (A14) is an artifact of the approximation (A6); if we do not project the momenta onto the Fermi surface, the resulting integral in Eq. (A4) depends only logarithmically on the ultraviolet cutoff, which follows from the fact that for large $|\mathbf{q}|$ the static polarization $\Pi_0(\mathbf{q}, 0)$ vanishes as $1/q^2$.

Finally, let us evaluate the term $\Phi_1(P=0)$ defined in Eq. (2.25), which contributes to the shift of T_c if we fix the chemical potential instead of the density. Therefore we manipulate the right-hand side of Eq. (2.25) for $P=0$ as follows,

$$\begin{aligned} \Phi_1(0) &= -2g\rho_0 \int_K G_0^2(K)G_0(-K) \\ &= -2g\rho_0 \int_K \frac{1}{(i\omega - \xi_{\mathbf{k}})^2(-i\omega - \xi_{\mathbf{k}})} \\ &= -g\rho_0 \int_K \frac{\partial}{\partial \xi_{\mathbf{k}}} \frac{1}{(i\omega - \xi_{\mathbf{k}})(-i\omega - \xi_{\mathbf{k}})} \\ &= -g\rho_0 \int_{\mathbf{k}} \frac{\partial}{\partial \xi_{\mathbf{k}}} \frac{\tanh(\frac{\beta}{2}\xi_{\mathbf{k}})}{2\xi_{\mathbf{k}}} \\ &= g\rho_0 \int_0^{\infty} d\epsilon \frac{\partial \nu(\epsilon)}{\partial \epsilon} \frac{\tanh(\frac{\beta}{2}(\epsilon - \mu))}{2(\epsilon - \mu)}, \end{aligned} \quad (\text{A15})$$

where we have integrated by parts to express the integral in terms of the derivative of the energy-dependent density of states $\nu(\epsilon)$. Using the fact that in D dimensions the density (per spin projection) can be related to the density of states at the Fermi energy as $\rho_0 = (2/D)\nu/E_F$, we obtain in three dimensions to leading logarithmic order

$$\Phi_1(0) = \frac{g\nu}{3} \Phi_0(0) = \frac{g\nu^2}{3} [\ln(A/\tau) + \lambda_0], \quad (\text{A16})$$

in agreement with Eq. (2.32).

APPENDIX B: FRG FLOW OF INDUCED INTERACTIONS

The vertex expansion (3.3) of the generating functional $\Gamma_{\Lambda}[\bar{c}, c, \bar{\psi}, \psi]$ of the irreducible vertices contains four different types of four-point vertices, which are defined graphically in Fig. 3. In our interaction-momentum cutoff scheme, only the effective two-body interaction $\Gamma_{\Lambda}^{\bar{\psi}\bar{\psi}\psi\psi}(P'_1, P'_2; P_2, P_1)$ between superfluid fluctuations shown in Fig. 3 (d) is finite at the initial scale. The exact FRG equation for this vertex is given in Eq. (3.17) and is shown graphically in Fig. 9. In this appendix, we give the exact FRG flow equations for the other three induced interaction vertices shown in Fig. 3.

In Fig. 17 we show a graphical representation of the exact FRG flow equation of the induced fermion-boson interaction vertex $\Gamma_{\Lambda}^{\bar{c}\sigma c\sigma\bar{\psi}\psi}(K', K; P', P)$ in our interaction-momentum cutoff scheme. For our purpose, we need only a truncated version of this flow equation where all vertices which vanish at the initial scale are neglected on the right-hand side of the flow equations. In this limit we obtain the FRG flow equation shown graphically in Fig. 10 (a),

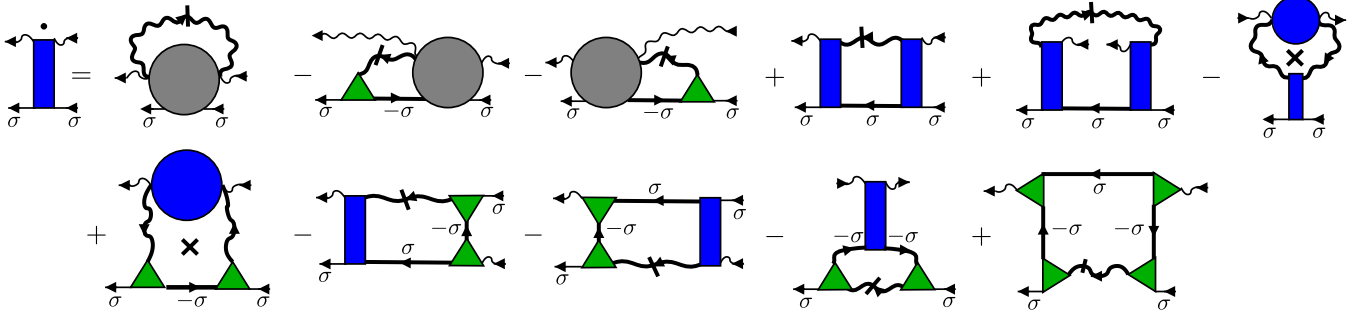


FIG. 17. Graphical representation of the exact FRG flow equation for the induced fermion-boson interaction vertex $\Gamma_{\Lambda}^{\bar{c}\sigma c\sigma\bar{\psi}\psi}(K', K; P', P)$. The cross in the last diagram of the first line and the first diagram in the second line corresponds to the product rule notation Eq. (3.18).

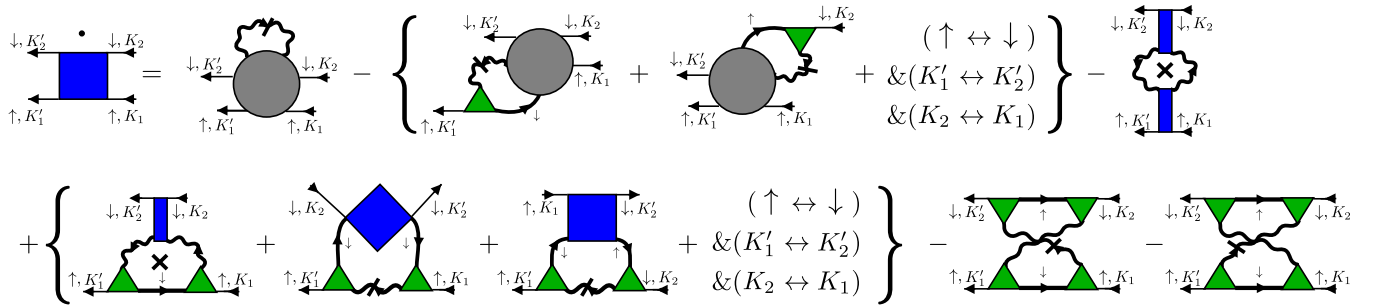


FIG. 18. Graphical representation of the exact FRG flow equation for the induced fermion interaction $\Gamma_{\Lambda}^{\bar{c}\uparrow\bar{c}\downarrow c\downarrow c\uparrow}(K'_1, K'_2; K_2, K_1)$ between electrons with opposite spin. The cross in the last diagram of the first line and the first diagram of the second line corresponds to our product rule notation. The permutations of the external labels have to be applied on all diagrams in the curly braces. Vertices are antisymmetric under permutation of two external fermionic legs corresponding to fields of the same kind.

which is explicitly given by

$$\begin{aligned}
\partial_{\Lambda}\Gamma_{\Lambda}^{\bar{c}\sigma c\sigma\bar{\psi}\psi}(K'_1, K_1; P'_1, P_1) &= \int_P \dot{F}_{\Lambda}(P)G_{\Lambda}(P - K'_1)G_{\Lambda}(P - K_1)G_{\Lambda}(P_1 + K_1 - P) \\
&\quad \times \Gamma_{\Lambda}^{\bar{c}\sigma\bar{c}-\sigma\psi}(K'_1, P - K'_1; P)\Gamma_{\Lambda}^{c-\sigma c\sigma\bar{\psi}}(P - K'_1, P_1 + K_1 - P; P'_1) \\
&\quad \times \Gamma_{\Lambda}^{\bar{c}\sigma\bar{c}-\sigma\psi}(P_1 + K_1 - P, P - K_1; P_1)\Gamma_{\Lambda}^{c-\sigma c\sigma\bar{\psi}}(P - K_1, K_1; P) \\
&\quad + \int_P [F_{\Lambda}(P)F_{\Lambda}(P + K_1 - K'_1)]^{\bullet} \Gamma_{\Lambda}^{\bar{\psi}\psi\psi\psi}(P'_1, P; P + K_1 - K'_1, P_1) \\
&\quad \times \Gamma_{\Lambda}^{\bar{c}\sigma\bar{c}-\sigma\psi}(K'_1, P - K'_1; P)\Gamma_{\Lambda}^{c-\sigma c\sigma\bar{\psi}}(P - K'_1, K_1; P + K_1 - K'_1). \tag{B1}
\end{aligned}$$

Here we have used the product rule notation introduced in Eq. (3.18),

$$[F_{\Lambda}(P)F_{\Lambda}(P')]^{\bullet} = \dot{F}_{\Lambda}(P)F_{\Lambda}(P') + F_{\Lambda}(P)\dot{F}_{\Lambda}(P'). \tag{B2}$$

Next, consider for completeness the FRG flow equations for the two types of purely fermionic induced interaction vertices defined in Fig. 3 (a) and (b). Since these flow equations are rather lengthy, we do not explicitly write them down here but represent them graphically in Fig. 18 and Fig. 19. We can close the infinite hierarchy of FRG flow equations by neglecting all vertices with more than four external legs on right-hand side. Then the FRG flow equation for the induced interaction between two electrons with opposite spin reduces to

$$\begin{aligned}
&\partial_{\Lambda}\Gamma_{\Lambda}^{\bar{c}\uparrow\bar{c}\downarrow c\downarrow c\uparrow}(K'_1, K'_2; K_2, K_1) \\
&\approx - \int_P [F_{\Lambda}(P)F_{\Lambda}(P - K_2 + K'_2)]^{\bullet} \Gamma_{\Lambda}^{\bar{c}\downarrow c\uparrow\bar{\psi}\psi}(K'_2; K_2; P; P - K_2 + K'_2)\Gamma_{\Lambda}^{\bar{c}\uparrow c\uparrow\bar{\psi}\psi}(K'_1; K_1; P - K_2 + K'_2; P)
\end{aligned}$$

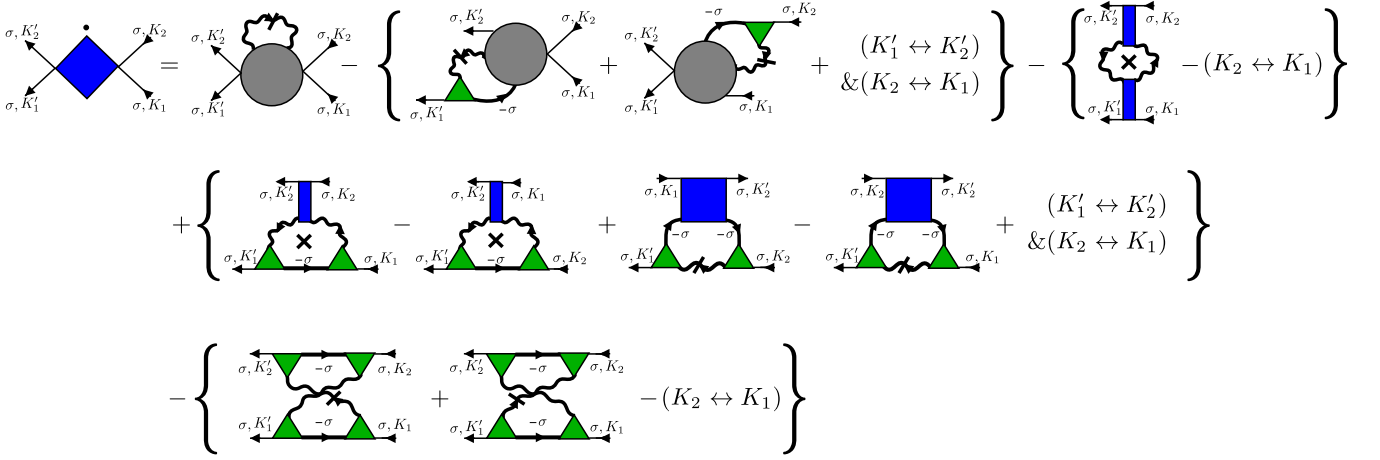


FIG. 19. The flow equation for the induced fermion interaction $\Gamma_{\Lambda}^{\bar{c}\sigma c\sigma c\sigma}(K'_1, K'_2; K_2, K_1)$ between electrons with parallel spin. The permutations of the external labels have to be applied on all diagrams in the curly braces. The cross in the last two diagrams of the first line and the second two diagrams of the second line correspond to our product rule notation. Vertices are antisymmetric under permutation of two external fermionic legs corresponding to fields of the same kind

$$\begin{aligned}
& + \left\{ \int_P [F_{\Lambda}(P)F_{\Lambda}(P - K'_1 + K_1)]^{\bullet} G_{\Lambda}(P - K'_1) \Gamma_{\Lambda}^{\bar{c}_1 c_1 \bar{\psi} \psi}(K'_2; K_2; P; P - K'_1 + K_1) \right. \\
& \quad \times \Gamma_{\Lambda}^{c_1 c_{\uparrow} \bar{\psi}}(P - K'_1, K_1; P - K'_1 + K_1) \Gamma_{\Lambda}^{\bar{c}_{\uparrow} \bar{c}_{\downarrow} \psi}(K'_1, P - K'_1; P) \\
& + \int_P \dot{F}_{\Lambda}(P) G_{\Lambda}(P - K_1) G_{\Lambda}(P - K'_1) \Gamma_{\Lambda}^{\bar{c}_{\downarrow} \bar{c}_{\uparrow} c_{\downarrow} c_{\uparrow}}(P - K_1, K'_2; P - K'_1, K_2) \\
& \quad \times \Gamma_{\Lambda}^{c_{\downarrow} c_{\uparrow} \bar{\psi}}(P - K_1, K_1; P) \Gamma_{\Lambda}^{\bar{c}_{\uparrow} \bar{c}_{\downarrow} \psi}(K'_1, P - K'_1; P) \\
& + \int_P \dot{F}_{\Lambda}(P) G_{\Lambda}(P - K'_1) G_{\Lambda}(P - K_2) \Gamma_{\Lambda}^{\bar{c}_{\uparrow} \bar{c}_{\downarrow} c_{\downarrow} c_{\uparrow}}(P - K_2, K'_2; P - K'_1, K_1) \\
& \quad \times \Gamma_{\Lambda}^{c_{\downarrow} c_{\uparrow} \bar{\psi}}(K_2, P - K_2; P) \Gamma_{\Lambda}^{\bar{c}_{\uparrow} \bar{c}_{\downarrow} \psi}(K'_1, P - K'_1; P) \\
& \left. + [(\uparrow \leftrightarrow \downarrow) \&(K'_1 \leftrightarrow K'_2) \&(K_2 \leftrightarrow K_1)] \right\} \\
& - \int_P [F_{\Lambda}(P)F_{\Lambda}(P - K'_1 + K_1)]^{\bullet} G_{\Lambda}(P - K'_1) G_{\Lambda}(P - K_2) \Gamma_{\Lambda}^{\bar{c}_{\uparrow} \bar{c}_{\downarrow} \psi}(K'_1, P - K'_1; P) \\
& \quad \times \Gamma_{\Lambda}^{c_{\downarrow} c_{\uparrow} \bar{\psi}}(P - K'_1, K_1; P - K'_1 + K_1) \Gamma_{\Lambda}^{\bar{c}_{\uparrow} \bar{c}_{\downarrow} \psi}(P - K_2, K'_2; P + K_1 - K'_1) \Gamma_{\Lambda}^{c_{\downarrow} c_{\uparrow} \bar{\psi}}(K_2, P - K_2; P), \quad (B3)
\end{aligned}$$

while the flow of effective interaction between electrons with parallel spin is given by

$$\begin{aligned}
& \partial_{\Lambda} \Gamma_{\Lambda}^{\bar{c}\sigma c\sigma c\sigma}(K'_1, K'_2; K_2, K_1) \\
& \approx \int_P [F_{\Lambda}(P)F_{\Lambda}(P - K'_2 + K_1)]^{\bullet} \Gamma_{\Lambda}^{\bar{c}\sigma c\sigma \bar{\psi} \psi}(K'_2; K_1; P - K'_2 + K_1; P) \Gamma_{\Lambda}^{\bar{c}\sigma c\sigma \bar{\psi} \psi}(K'_1; K_2; P; P - K'_2 + K_1) \\
& - \int_P [F_{\Lambda}(P)F_{\Lambda}(P - K_2 + K'_2)]^{\bullet} \Gamma_{\Lambda}^{\bar{c}\sigma c\sigma \bar{\psi} \psi}(K'_2; K_2; P; P - K_2 + K'_2) \Gamma_{\Lambda}^{\bar{c}\sigma c\sigma \bar{\psi} \psi}(K'_1; K_1; P - K_2 + K'_2; P) \\
& + \left\{ \int_P [F_{\Lambda}(P)F_{\Lambda}(P - K'_1 + K_1)]^{\bullet} G_{\Lambda}(P - K'_1) \Gamma_{\Lambda}^{\bar{c}\sigma c\sigma \bar{\psi} \psi}(K'_2; K_2; P; P - K'_1 + K_1) \right. \\
& \quad \times \Gamma_{\Lambda}^{c - \sigma c\sigma \bar{\psi}}(P - K'_1, K_1; P - K'_1 + K_1) \Gamma_{\Lambda}^{\bar{c}\sigma \bar{c} - \sigma \psi}(K'_1, P - K'_1; P) \\
& - \int_P [F_{\Lambda}(P)F_{\Lambda}(P - K'_1 + K_2)]^{\bullet} G_{\Lambda}(P - K'_1) \Gamma_{\Lambda}^{\bar{c}\sigma c\sigma \bar{\psi} \psi}(K'_2, K_1; P, P - K'_1 + K_2) \\
& \quad \times \Gamma_{\Lambda}^{c - \sigma c\sigma \bar{\psi}}(P - K'_1, K_2; P - K'_1 + K_2) \Gamma_{\Lambda}^{\bar{c}\sigma \bar{c} - \sigma \psi}(K'_1, P - K'_1; P) \\
& - \int_P \dot{F}_{\Lambda}(P) G_{\Lambda}(P - K_1) G_{\Lambda}(P - K'_1) \Gamma_{\Lambda}^{\bar{c}\sigma c\sigma c\sigma c - \sigma}(P - K_1, K'_2; K_2, P - K'_1) \\
& \quad \times \Gamma_{\Lambda}^{c - \sigma c\sigma \bar{\psi}}(P - K_1, K_1; P) \Gamma_{\Lambda}^{\bar{c}\sigma \bar{c} - \sigma \psi}(K'_1, P - K'_1; P)
\end{aligned}$$

$$\begin{aligned}
& + \int_P \dot{F}_\Lambda(P) G_\Lambda(P - K'_1) G_\Lambda(P - K_2) \Gamma_\Lambda^{\bar{c}-\sigma \bar{c} \sigma c \sigma c - \sigma}(P - K_2, K'_2; K_1, P - K'_1) \\
& \quad \times \Gamma_\Lambda^{c-\sigma c \sigma \bar{\psi}}(P - K_2, K_2; P) \Gamma_\Lambda^{\bar{c} \sigma \bar{c} - \sigma \psi}(K'_1, P - K'_1; P) \\
& \quad + [(\uparrow \leftrightarrow \downarrow) \&(K'_1 \leftrightarrow K'_2) \&(K_2 \leftrightarrow K_1)] \Big\} \\
& - \int_P [F_\Lambda(P) F_\Lambda(P - K'_1 + K_1)]^\bullet G_\Lambda(P - K'_1) G_\Lambda(P - K_2) \Gamma_\Lambda^{\bar{c} \sigma \bar{c} - \sigma \psi}(K'_1, P - K'_1; P) \\
& \quad \times \Gamma_\Lambda^{c-\sigma c \sigma \bar{\psi}}(P - K'_1, K_1; P - K'_1 + K_1) \Gamma_\Lambda^{\bar{c} - \sigma \bar{c} \sigma \psi}(P - K_2, K'_2; P + K_1 - K'_1) \Gamma_\Lambda^{c \sigma c - \sigma \bar{\psi}}(K_2, P - K_2; P) \\
& + \int_P [F_\Lambda(P) F_\Lambda(P - K'_1 + K_2)]^\bullet G_\Lambda(P - K'_1) G_\Lambda(P - K_1) \Gamma_\Lambda^{\bar{c} \sigma \bar{c} - \sigma \psi}(K'_1, P - K'_1; P) \\
& \quad \times \Gamma_\Lambda^{c-\sigma c \sigma \bar{\psi}}(P - K_1, K_1; P) \Gamma_\Lambda^{\bar{c} \sigma \bar{c} - \sigma \psi}(K'_2, P - K_1; P - K'_1 + K_2) \Gamma_\Lambda^{c-\sigma c \sigma \bar{\psi}}(P - K'_1, K_2; P - K'_1 + K_2). \quad (B4)
\end{aligned}$$

As a first step in an iterative solution of these flow equations, we may set all vertices which vanish at the initial scale equal to zero. Then the FRG flow equation (B3) for the effective interaction between electrons with opposite spin reduces to

$$\begin{aligned}
\partial_\Lambda \Gamma_\Lambda^{\bar{c} \uparrow \bar{c} \downarrow c \uparrow c \uparrow}(K'_1, K'_2; K_2, K_1) & \approx - \int_K [F_\Lambda(K + K_2) F_\Lambda(K + K'_2)]^\bullet G_\Lambda(K) G_\Lambda(K + K_2 - K'_1) \\
& \quad \times \Gamma_\Lambda^{\bar{c} \uparrow \bar{c} \downarrow \psi}(K'_1, K + K_2 - K'_1; K + K_2) \Gamma_\Lambda^{c \downarrow c \uparrow \bar{\psi}}(K + K_2 - K'_1, K_1; K + K'_2) \\
& \quad \times \Gamma_\Lambda^{c \downarrow c \uparrow \bar{\psi}}(K_2, K; K + K_2) \Gamma_\Lambda^{\bar{c} \uparrow \bar{c} \downarrow \psi}(K, K'_2; K + K'_2), \quad (B5)
\end{aligned}$$

which is shown graphically in Fig. 10 (b). Another approximation strategy is to replace the three-point and bosonic four-point vertices on the right-hand sides of the flow equations in Fig. 10 by their initial values $\Gamma_\Lambda^{\bar{c} \uparrow \bar{c} \downarrow \psi} = \Gamma_\Lambda^{c \downarrow c \uparrow \bar{\psi}} \approx 1$ and $\Gamma_\Lambda^{\bar{\psi} \bar{\psi} \psi \psi} \approx \Gamma_{\Lambda_0}^{\bar{\psi} \bar{\psi} \psi \psi}$. Then the FRG flow of the mixed boson-fermion interaction reduces to

$$\begin{aligned}
& \partial_\Lambda \Gamma_\Lambda^{\bar{c} \sigma c \sigma \bar{\psi} \psi}(K'_1; K_1; P'_1; P_1) \\
& = \int_P \dot{F}_\Lambda(P) G_\Lambda(P - K'_1) G_\Lambda(P - K_1) G_\Lambda(P_1 + K_1 - P) \\
& + \int_P [F_\Lambda(P) F_\Lambda(P + K_1 - K'_1)]^\bullet \\
& \quad \times \Gamma_{\Lambda_0}^{\bar{\psi} \bar{\psi} \psi \psi}(P'_1, P; P + K_1 - K'_1, P_1), \quad (B6)
\end{aligned}$$

while the induced interaction between fermions with opposite spin determined by the truncated flow equation

$$\begin{aligned}
& \partial_\Lambda \Gamma_\Lambda^{\bar{c} \uparrow \bar{c} \downarrow c \downarrow c \uparrow}(K'_1, K'_2; K_2, K_1) \\
& = - \int_P [F_\Lambda(P) F_\Lambda(P + K_1 - K'_1)]^\bullet \\
& \quad \times G_\Lambda(P - K'_1) G_\Lambda(P + K_1 - K'_1 - K'_2). \quad (B7)
\end{aligned}$$

APPENDIX C: PARTICLE-PARTICLE BUBBLE AT FINITE MOMENTUM AND FREQUENCY

To calculate the expansion of the particle-particle bubble for small momenta and frequencies, it is convenient to expand in powers of external momenta and frequencies before carrying out the Matsubara sums. Therefore we

write Eq. (A1) as

$$\begin{aligned}
\Phi_0(\mathbf{p}, i\bar{\omega}) & = \int_K G_0(K) G_0(P - K) \\
& = T \sum_\omega \int_{\mathbf{k}} \frac{1}{i\omega - \xi_{\mathbf{k}}} \frac{1}{i\bar{\omega} - i\omega - \xi_{\mathbf{p}-\mathbf{k}}}. \quad (C1)
\end{aligned}$$

In the book by Larkin and Varlamov¹ one can find an approximate evaluation of Eq. (C1) in the regime $v_F p \ll T \ll E_F$ where the momentum integral is dominated by states with energies close to the Fermi energy. In this regime the energy dependence of the density of states $\nu(\epsilon)$ can be neglected so that we may approximate $\nu(\epsilon) \approx \nu(E_F) \equiv \nu$ under the integral. Using the T -matrix regularization defined via Eq. (2.19) we then obtain for the regularized particle-particle bubble

$$\begin{aligned}
\Phi_0^{\text{reg}}(\mathbf{p}, i\bar{\omega}) & \approx \nu \left[\ln \left(\frac{A E_F}{T} \right) + \psi \left(\frac{1}{2} \right) - \psi \left(\frac{1}{2} + \frac{|\bar{\omega}|}{4\pi T} \right) \right. \\
& \quad \left. + \frac{\langle (\mathbf{v}_F \cdot \mathbf{p})^2 \rangle}{2(4\pi T)^2} \psi'' \left(\frac{1}{2} + \frac{|\bar{\omega}|}{4\pi T} \right) \right], \quad (C2)
\end{aligned}$$

where for a spherical Fermi surface in D dimensions the Fermi surface average in Eq. (C2) is

$$\langle (\mathbf{v}_F \cdot \mathbf{p})^2 \rangle = \frac{v_F^2 p^2}{D}. \quad (C3)$$

The Digamma function $\psi(z)$ has the representation

$$\psi(z) = \frac{d \ln \Gamma(z)}{dz} = -\gamma_E + \sum_{n=0}^{\infty} \left[\frac{1}{n+1} - \frac{1}{n+z} \right], \quad (C4)$$

where $\gamma_E \approx 0.577$ is the Euler-Mascheroni constant. The numerical constant $A = 8/(\pi e^{2-\gamma_E})$ in the argument of the logarithm in Eq. (C2) has already been introduced in Eq. (2.29). Note that

$$\psi(1/2) = -\gamma_E - 2 \ln 2, \quad (\text{C5a})$$

$$\psi'(1/2) = 3\zeta(2) = \frac{\pi^2}{2}, \quad (\text{C5b})$$

$$\psi''(1/2) = -14\zeta(3) \approx -16.8, \quad (\text{C5c})$$

and that for large $|z|$ the Digamma function has the asymptotic expansion

$$\psi(z+1) \sim \ln z + \frac{1}{2z} + \mathcal{O}(z^{-2}). \quad (\text{C6})$$

The mean-field critical temperature T_{c0} is determined by

$$g^{-1} - \Phi_0^{\text{reg}}(0,0)|_{T_{c0}} = 0, \quad (\text{C7})$$

which yields the well-known weak-coupling result quoted in Eq. (2.30). Setting

$$\begin{aligned} r_0 &\equiv g^{-1} - \Phi_0^{\text{reg}}(0,0) = \Phi_0^{\text{reg}}(0,0)|_{T_{c0}} - \Phi_0^{\text{reg}}(0,0) \\ &\approx \nu \ln \left(\frac{T}{T_{c0}} \right) \approx \nu \frac{T - T_{c0}}{T_{c0}} \equiv \nu t_0, \end{aligned} \quad (\text{C8})$$

we see that in the weak coupling regime and for small momenta the inverse bosonic propagator can be written as

$$\begin{aligned} F_0^{-1}(\mathbf{p}, i\bar{\omega}) &= \nu \left[t_0 + \psi \left(\frac{1}{2} + \frac{|\bar{\omega}|}{4\pi T} \right) - \psi \left(\frac{1}{2} \right) \right. \\ &\quad \left. - \frac{v_F^2 p^2}{2D(4\pi T)^2} \psi'' \left(\frac{1}{2} + \frac{|\bar{\omega}|}{4\pi T} \right) \right]. \end{aligned} \quad (\text{C9})$$

The corresponding retarded propagator can be obtained via analytic continuation, $|\bar{\omega}| = -i(i\bar{\omega})\text{sgn}\bar{\omega} \rightarrow -i\omega$. Assuming $|\omega| \ll 4\pi T$ we may expand the Digamma functions in powers of frequencies and obtain for the inverse retarded propagator

$$F_0^{-1}(\mathbf{p}, \omega + i0^+) \approx \nu [t_0 - i\omega/\omega_0 + p^2/p_0^2], \quad (\text{C10})$$

where

$$\omega_0 = 8T/\pi, \quad (\text{C11})$$

and

$$p_0^2 = \frac{16D}{7\zeta(3)} \left(\frac{\pi T}{v_F} \right)^2 \quad (\text{C12})$$

can be identified with the square of the inverse coherence length. In particular, in the static limit the Gaussian propagator of the pairing field can be written as

$$F_0(\mathbf{p}, 0) \approx \frac{1}{\nu [t_0 + p^2/p_0^2]}. \quad (\text{C13})$$

The above expressions are only valid in the weak coupling BCS limit at low temperatures, where $\tilde{g} = \nu g \ll 1$,

$T \ll E_F$, and $p \lesssim p_0 \ll k_F$. On the other hand, when \tilde{g} is of the order of unity the energy dependence of the density of states cannot be neglected, so that Eq. (C2) is not valid. Setting for simplicity $\bar{\omega} = 0$ (which is sufficient for our purpose because we are only interested in classical long-wavelength fluctuations) we write the static propagator of the order parameter field as

$$F_0(\mathbf{p}, 0) = \frac{1}{r_0 + c_0 p^2}. \quad (\text{C14})$$

In the BCS limit we obtain from Eq. (C10)

$$r_0 \approx \nu t_0, \quad (\text{C15})$$

$$c_0 \approx \nu/p_0^2. \quad (\text{C16})$$

More generally, for arbitrary values of g the coefficients r_0 and c_0 can be obtained directly from Eq. (C1). For the parameter r_0 which measures the distance to the critical point we obtain

$$\begin{aligned} r_0 &= \Phi_0^{\text{reg}}(0,0)|_{T_c} - \Phi_0^{\text{reg}}(0,0) \\ &= \int_0^\infty d\epsilon \nu(\epsilon) \frac{\tanh(\frac{\epsilon-\mu}{2T_c}) - \tanh(\frac{\epsilon-\mu}{2T})}{2(\epsilon-\mu)} \\ &= \int_0^\infty d\epsilon \nu(\epsilon) \frac{\sinh(\frac{(\epsilon-\mu)t_0}{2T})}{2(\epsilon-\mu) \cosh(\frac{\epsilon-\mu}{2T_{c0}}) \cosh(\frac{\epsilon-\mu}{2T})}, \end{aligned} \quad (\text{C17})$$

where the energy-dependent density of states (per spin projection) is in three dimensions given by

$$\nu(\epsilon) = \int_{\mathbf{k}} \delta(\epsilon - \epsilon_{\mathbf{k}}) = \frac{m\sqrt{2m\epsilon}}{2\pi^2} = K_3 m \sqrt{2m\epsilon}. \quad (\text{C18})$$

Assuming $\mu > 0$ and introducing the dimensionless integration variable $x = \epsilon/\mu$ we obtain to leading order in the reduced temperature $t_0 = (T - T_{c0})/T_{c0}$,

$$r_0 = Z_r(\mu/T) \nu(\mu) t_0, \quad (\text{C19})$$

where the dimensionless function $Z_r(\alpha)$ is given by

$$Z_r(\alpha) = \frac{\alpha}{4} \int_0^\infty dx \frac{\sqrt{x}}{\cosh^2(\alpha \frac{x-1}{2})}. \quad (\text{C20})$$

In the BCS limit where $\mu \approx E_F \gg T$ we may approximate $Z_r(\mu/T) \approx Z_r(\infty) = 1$ and obtain $r_0 = \nu t_0$, in agreement with Eq. (C8). A graph of the function $Z_r(\mu/T)$ is shown in Fig. 20. Finally, consider the coefficient c_0 in Eq. (C14), which can be written as

$$\begin{aligned} c_0 &= - \left. \frac{\partial \Phi_0^{\text{reg}}(\mathbf{p}, 0)}{\partial p^2} \right|_{p=0} \\ &= \frac{T}{2m} \sum_{\omega} \int_{\mathbf{k}} \left[\frac{\frac{2}{D} \frac{k^2}{m}}{(i\omega - \xi_{\mathbf{k}})(i\omega + \xi_{\mathbf{k}})^3} \right. \\ &\quad \left. - \frac{1}{(i\omega - \xi_{\mathbf{k}})(i\omega + \xi_{\mathbf{k}})^2} \right]. \end{aligned} \quad (\text{C21})$$

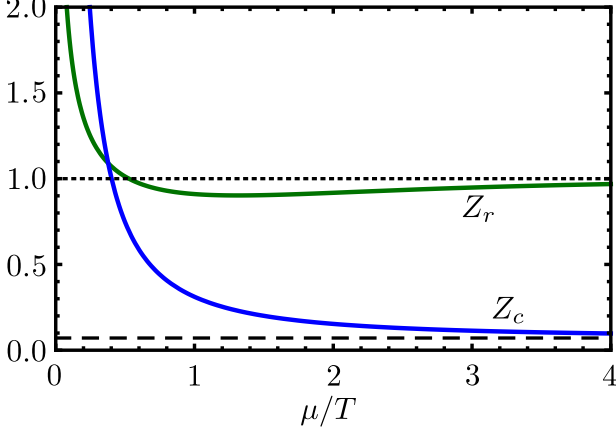


FIG. 20. Graph of the functions $Z_r(\alpha)$ and $Z_c(\alpha)$ defined in Eqs. (C20) and (C23). While for large $\alpha = \mu/T$ these functions approach finite constants, $Z_r(\infty) = 1$ and $Z_c(\infty) \approx 0.071$, the asymptotic behavior for $\alpha \rightarrow 0$ is $Z_r(\alpha) \propto \alpha^{-1/2}$ and $Z_c(\alpha) \propto \alpha^{-3/2}$.

After carrying out the Matsubara sums we obtain

$$c_0 = Z_c(\mu/T) \frac{\nu(\mu)\mu}{2mT^2}, \quad (\text{C22})$$

with

$$Z_c(\alpha) = \alpha \int_0^\infty dx \sqrt{x} \left\{ (x-1)S_2(\alpha(x-1)) + \frac{4}{3}x \left[S_2(\alpha(x-1)) - 2\alpha^2(x-1)^2 S_3(\alpha(x-1)) \right] \right\}. \quad (\text{C23})$$

Here $S_2(a)$ and $S_3(a)$ are defined by the following fermionic Matsubara sums,

$$S_2(a) = \sum_{n=-\infty}^{\infty} \frac{1}{[(\pi(2n+1))^2 + a^2]^2} = \frac{\sinh a - a}{8a^3 \cosh^2(a/2)}, \quad (\text{C24})$$

$$S_3(a) = \sum_{n=-\infty}^{\infty} \frac{1}{[(\pi(2n+1))^2 + a^2]^3} = \frac{1}{32a^5} \left[6 \tanh(a/2) - \frac{3a}{\cosh^2(a/2)} - \frac{8a^2 \sinh^4(a/2)}{\sinh^3 a} \right]. \quad (\text{C25})$$

A graph of the function $Z_c(\alpha)$ is shown in Fig. 20. In the BCS limit where $\mu/T \gg 1$ we obtain to leading order in D dimensions

$$Z_c(\mu/T) \sim Z_c(\infty) = \frac{7\zeta(3)}{4\pi^2 D}. \quad (\text{C26})$$

APPENDIX D: JUSTIFICATION OF THE CLASSICAL APPROXIMATION CLOSE TO T_c

To justify the static approximation for pairing fluctuations in the evaluation of the electronic self-energy given in Eq. (4.7) we go back to Eq. (4.1), introduce the spectral representation of the Gaussian pairing propagator, and explicitly carry out the Matsubara sum. Therefore it is useful to write the Gaussian pairing propagator as

$$F_0(P) = \frac{g_0}{1 - g_0 \Phi_0(P)} = g_0 + g_0^2 \frac{\Phi_0(P)}{1 - g_0 \Phi_0(P)}. \quad (\text{D1})$$

Given the fact that particle-particle bubble $\Phi_0(\mathbf{p}, i\bar{\omega})$ vanishes for large $|\bar{\omega}|$ as $1/|\bar{\omega}|$ we see that the corresponding resummed bubble $\Phi_0(P)/[1 - g_0 \Phi_0(P)]$ vanishes also for large $|\bar{\omega}|$, so that it has a spectral representation

$$\frac{\Phi_0(\mathbf{p}, i\bar{\omega})}{1 - g_0 \Phi_0(\mathbf{p}, i\bar{\omega})} = \int_{-\infty}^{\infty} d\omega' \frac{S(\mathbf{p}, \omega')}{\omega' - i\bar{\omega}}. \quad (\text{D2})$$

The inverse relation is

$$S(\mathbf{p}, \omega) = \frac{1}{\pi} \text{Im} \left[\frac{\Phi_0(\mathbf{p}, \omega + i0^+)}{1 - g_0 \Phi_0(\mathbf{p}, \omega + i0^+)} \right]. \quad (\text{D3})$$

From the expansion (C10) we see that for small frequencies $|\omega| \ll T$,

$$\frac{\Phi_0(\mathbf{p}, \omega + i0^+)}{1 - g_0 \Phi_0(\mathbf{p}, \omega + i0^+)} \approx \frac{1}{\nu g_0^2} \frac{1}{t_0 - i\omega/\omega_0 + c_0 p^2}, \quad (\text{D4})$$

where in the BCS regime $\omega_0 = 8T/\pi$ and $p_0 = \sqrt{3/(7\zeta(3))} 4\pi T/v_F$, see Eqs. (C11) and (C12). The spectral function is therefore

$$S(\mathbf{p}, \omega) = \frac{1}{\pi \nu g_0^2} \frac{\omega/\omega_0}{(\omega/\omega_0)^2 + (t_0 + p^2/p_0^2)^2}. \quad (\text{D5})$$

Substituting Eqs. (D1) and (D2) into Eq. (4.1) we may carry out the Matsubara sum and obtain

$$\Sigma(\mathbf{k}, i\omega) = -g_0 \rho_0 + g_0^2 \int_{\mathbf{p}} \int_{-\infty}^{\infty} d\omega' S(\mathbf{p}, \omega') \times \frac{b(\omega') + f(\xi_{\mathbf{p}-\mathbf{k}}) - 1}{i\omega - \omega' + \xi_{\mathbf{p}-\mathbf{k}}}. \quad (\text{D6})$$

Here $b(\omega') = 1/[e^{\omega'/T} - 1]$ is the Bose function and $f(\xi) = 1/[e^{\xi/T} + 1]$ is the Fermi function. From this expression we can now justify the static approximation for temperatures close to T_c . In this regime, the dynamics of the boson is much slower than the dynamics of the fermions because the typical value of the boson frequency is $\omega' \approx \omega_0(t_0 + p^2/p_0^2)$, whereas the typical value of the fermion energy is of order $v_F p \ll T$. In this regime we may approximate the Bose function by its classical limit $b(\omega') \approx T/\omega'$ and neglect the term $f(\xi_{\mathbf{p}-\mathbf{k}}) - 1$ and the constant $-g_0 n$. In this approximation

$$\Sigma(\mathbf{k}, i\omega) = g_0^2 \int_{\mathbf{p}} \int_{-\infty}^{\infty} d\omega' \frac{S(\mathbf{p}, \omega')}{\omega'} \frac{T}{i\omega + \xi_{\mathbf{p}-\mathbf{k}}}.$$

(D7)

By definition the frequency integral gives

$$\int_{-\infty}^{\infty} d\omega' \frac{S(\mathbf{p}, \omega')}{\omega'} = \frac{\Phi_0(\mathbf{p}, 0)}{1 - g_0 \Phi_0(\mathbf{p}, 0)}. \quad (\text{D8})$$

For $p \ll T/v_F$ we may approximate in the numerator $\Phi_0(\mathbf{p}, 0) \approx 1/g_0$ so that we finally arrive at Eq. (4.7).

APPENDIX E: FRG CALCULATION WITH VERTEX CORRECTIONS

In the FRG calculation of the quasi-particle damping presented in Sec. IV B we have set the mixed fermion-boson interaction $\Gamma_{\Lambda}^{\bar{c}_{\sigma} c_{\sigma} \bar{\psi} \psi}(K', K; P', P)$ equal to zero and ignored the FRG flow of the three-point vertices $\Gamma_{\Lambda}^{\bar{c}_{\uparrow} \bar{c}_{\downarrow} \psi}(K'_1, K'_2; P)$ and $\Gamma_{\Lambda}^{c_{\downarrow} c_{\uparrow} \bar{\psi}}(K_1, K_2; P)$. However, if we assume the usual Fermi liquid scaling in the fermionic sector and Gaussian critical scaling in the bosonic sector, it is easy to see that the coupling

$$\begin{aligned} & \Gamma_{\Lambda}^{\bar{c}_{\uparrow} \bar{c}_{\downarrow} \psi}(\mathbf{k}_F, i0^+, -\mathbf{k}_F, -i0^+; 0, 0) \\ &= \Gamma_{\Lambda}^{c_{\downarrow} c_{\uparrow} \bar{\psi}}(-\mathbf{k}_F, -i0^+, \mathbf{k}_F, i0^+; 0, 0) \equiv v_{\Lambda} \end{aligned} \quad (\text{E1})$$

is relevant at the critical point with scaling dimension $2 - D/2 = 1/2$ in three dimensions. In the above definition of v_{Λ} it is understood that the bosonic momenta and frequencies are set equal to zero, while the fermionic frequency is analytically continued to the real axis and then set equal to zero with an infinitesimal imaginary part as indicated. Similarly, the coupling w_{Λ} defined by

$$\Gamma_{\Lambda}^{\bar{c}_{\sigma} c_{\sigma} \bar{\psi} \psi}(\mathbf{k}_F, \pm i0^+, \mathbf{k}_F, \pm i0^+; 0, 0) \equiv \pm i w_{\Lambda} \quad (\text{E2})$$

has scaling dimensions $3 - D$ and is therefore marginal in three dimensions. Hence, for the calculation of the feedback of critical order parameter fluctuations on the electronic properties, the RG flow of these two couplings has to be taken into account. If we neglect all other (irrelevant) vertices, the RG flow of w_{Λ} is given by the truncated flow equation shown graphically in Fig. 10 (a), which is explicitly written down in Eq. (B1). Introducing the dimensionless rescaled couplings

$$\tilde{v}_l = \sqrt{\frac{K_3 T}{v_F^2 c_{\Lambda} \Lambda}} v_{\Lambda} \quad (\text{E3})$$

$$\tilde{w}_l = \frac{K_3 T}{v_F c_{\Lambda}} w_{\Lambda}, \quad (\text{E4})$$

and the rescaled damping

$$\tilde{\gamma}_l = \frac{\gamma_{\Lambda}}{v_F \Lambda}, \quad (\text{E5})$$

we find that Eq. (B1) reduces to

$$\partial_l \tilde{w}_l = -\eta_l \tilde{w}_l + \frac{\tilde{v}_l^4}{2(1 + \tilde{r}_l) \tilde{\gamma}_l^2} \left[\arctan(1/\tilde{\gamma}_l) + \frac{\tilde{\gamma}_l}{1 + \tilde{\gamma}_l^2} \right]$$

$$+ \frac{\tilde{w}_l \tilde{v}_l^2}{(1 + \tilde{r}_l)^2} \arctan(1/\tilde{\gamma}_l). \quad (\text{E6})$$

Similarly, we obtain from the FRG flow equations for the three-point vertices given in Eqs. (3.15, 3.16) which are shown graphically in Fig. 10 (b),

$$\partial_l \tilde{v}_l = \frac{1 - \eta_l}{2} \tilde{v}_l + \frac{2\tilde{v}_l \tilde{w}_l}{1 + \tilde{r}_l} \arctan(1/\tilde{\gamma}_l). \quad (\text{E7})$$

Taking into account the couplings v_{Λ} and w_{Λ} , we obtain from Eq. (3.12) for the flow of the quasiparticle damping,

$$\partial_{\Lambda} \gamma_{\Lambda} = K_3 T \left[\frac{w_{\Lambda} \Lambda^2}{r_{\Lambda} + c_{\Lambda} \Lambda^2} - \frac{\Lambda v_{\Lambda}^2 \arctan(v_F \Lambda / \gamma_{\Lambda})}{v_F (r_{\Lambda} + c_{\Lambda} \Lambda^2)} \right]. \quad (\text{E8})$$

In terms of the rescaled couplings introduced above this can be written as

$$\partial_l \tilde{\gamma}_l = \tilde{\gamma}_l - \frac{\tilde{w}_l}{1 + \tilde{r}_l} + \frac{\tilde{v}_l^2 \arctan(1/\tilde{\gamma}_l)}{1 + \tilde{r}_l}. \quad (\text{E9})$$

The above system of flow equations should be integrated with the following initial conditions,

$$\Lambda_0 = p_0 \propto \frac{T}{v_F}, \quad (\text{E10})$$

$$\tilde{u}_0 = \frac{K_3 T u_0}{c_0^2 \Lambda_0} \propto \left(\frac{T}{E_F} \right)^2, \quad (\text{E11})$$

$$\tilde{v}_0 = \sqrt{\frac{K_3 T}{c_0 v_F^2 \Lambda_0}} \propto \frac{T}{E_F}, \quad (\text{E12})$$

$$\tilde{w}_0 = 0, \quad (\text{E13})$$

$$\tilde{\gamma}_0 = \frac{\gamma_{\text{FL}}}{v_F p_0} \propto \frac{T}{E_F}. \quad (\text{E14})$$

The finite initial value of $\tilde{\gamma}_l$ takes into account the usual Fermi liquid contribution to the quasi-particle damping which is not related to critical pairing fluctuations, see the discussion in Sec. IV A. For our model defined in Eq. (2.1) second order perturbation theory in the regularized interaction g yields for the quasiparticle damping at low temperatures⁶⁵

$$\gamma_{\text{FL}} = \frac{m^3}{8\pi} g^2 T^2 = \frac{\pi^2}{4} \tilde{g}^2 T^2 / E_F. \quad (\text{E15})$$

More generally, we may use the generic form of the quasi-particle damping of a Fermi liquid $\gamma_{\text{FL}} = C_{\text{FL}} T^2 / E_F$ [see Eq. (4.18)], where the value of the numerical constant C_{FL} is determined by all types of interaction processes into account, including those which are not included in our effective low-energy model (2.1). For simplicity we choose C_{FL} such that the initial condition for the rescaled damping is given by $\tilde{\gamma}_0 = T/E_F$.

After solving the flow equations (4.45–4.47) in the bosonic sector for various temperatures, we may substitute the result into the flow equations (E6) and (E7) for the four-legged and three-legged vertices, and into the flow equation (E9) for the quasiparticle damping. In

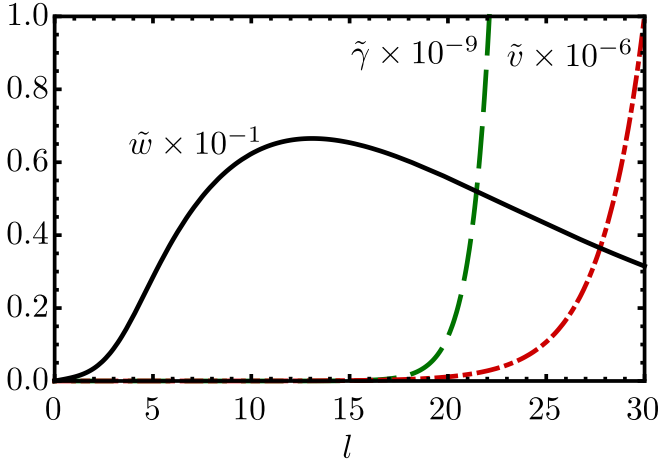


FIG. 21. RG flow of the rescaled damping $\tilde{\gamma}_l$ (green dashed line), three-legged vertex \tilde{v}_l (red dashed-dotted line), and mixed four-legged vertex \tilde{w}_l (black solid line) for $T = T_c = 0.13E_F$. For large l the rescaled damping $\tilde{\gamma}_l$ is proportional to e^l , so that $e^{-l}\tilde{\gamma}_l$ approaches a finite limit.

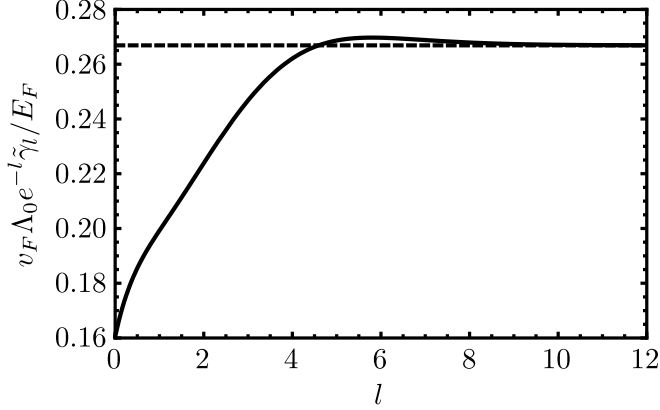


FIG. 22. RG flow of the physical damping $\gamma_\Lambda = v_F \Lambda \tilde{\gamma}_l$ as a function of $l = \ln(\Lambda_0/\Lambda)$ for $T = T_c = 0.13E_F$. The damping converges against a constant value for large l (dashed black line).

Fig. 21 we plot the flow of the rescaled couplings \tilde{v}_l and \tilde{w}_l as well as the rescaled quasiparticle damping $\tilde{\gamma}_l$ for $T = T_c = 0.13E_F$. From the solution for the dimensionless rescaled damping $\tilde{\gamma}_l$ we can reconstruct the physical quasiparticle damping due classical pairing parameter fluctuations as follows,

$$\gamma_{\text{crit}}(T) = v_F \Lambda_0 \lim_{l \rightarrow \infty} e^{-l} \tilde{\gamma}_l - \gamma_{\text{FL}}, \quad (\text{E16})$$

where the subtraction of the initial condition $\gamma_{\text{FL}} = v_F \Lambda_0 \tilde{\gamma}_0$ is necessary to isolate the contribution from classical pairing fluctuations. The rescaled damping $\tilde{\gamma}_l$ is proportional to $\propto e^l$ for large l , so that $e^{-l}\tilde{\gamma}_l$ converges against a constant value, as shown in Fig. 22. Our final result for the contribution from classical critical fluctuations to the quasi-particle damping $\gamma_{\text{crit}}(T_c)$ at the T_c is shown in Fig. 23, where we also show the corre-

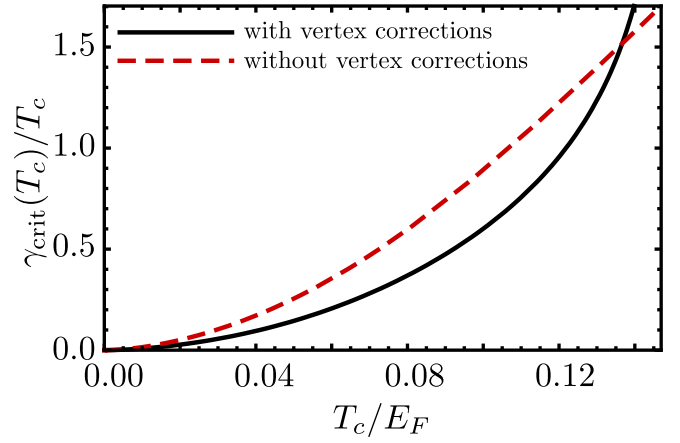


FIG. 23. The black solid line represents our numerical result for the damping $\gamma_{\text{crit}}(T_c)$ due to classical critical pairing fluctuations including vertex corrections, while the red dashed line is the corresponding result without vertex corrections discussed in Sec. IV B.

sponding expression without vertex corrections derived in Sec. IV B. Comparing the two curves we can see, that in the weak coupling limit $T_c \ll E_F$ the qualitative behavior is not modified by vertex corrections, while for larger values of the interaction (corresponding to $T_c \approx 0.1E_F$) vertex corrections do have a significant effect. One should keep in mind, however, that in the derivation of the flow equations (E6) and (E7) we have made several simplifications (for example, we have projected all external momenta of the vertices on the Fermi surface) which can only be expected to be quantitatively accurate in the weak coupling BCS regime. Hence, quantitative accuracy of our FRG calculation including vertex corrections can only be expected for $T_c/E_F \ll 1$. In this regime our FRG result for the quasiparticle damping shown in Fig. 23 can be fitted by

$$\gamma_{\text{crit}}(T_c) \approx C \frac{T_c^3}{E_F^2} \ln(E_F/T_c), \quad (\text{E17})$$

with $C \approx 18$. The above weak-coupling result including vertex corrections confirms our result of Sec. IV B given in Eq. (4.52). Note, however, that vertex corrections reduce the numerical value of the prefactor C from 34 to 18, which is still large compared with unity. A controlled calculation of the precise numerical value of C is beyond the scope of this work; in the calculation including vertex corrections of the numerical value of C is also sensitive to the choice of the numerical coefficient C_{FL} in the expression for the Fermi liquid damping $\gamma_{\text{FL}} = C_{\text{FL}} T^2/E_F$ defining the initial condition for the FRG flow equations.

Finally, let us point out that our FRG calculation predicts that at the critical point the marginal part w_Λ of the mixed four-point vertex defined in Eq. (E2) diverges logarithmically for vanishing cutoff $\Lambda \rightarrow 0$, while the relevant part v_Λ of the three-legged vertex approaches a finite value in this limit. To see this, we plot these unrescaled couplings in Fig. 24 for $T = T_c = 0.13E_F$ as

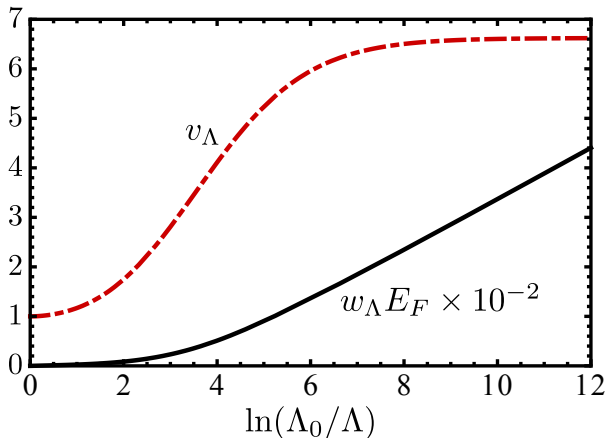


FIG. 24. RG flow of the physical couplings v_Λ and w_Λ as a function of $l = \ln(\Lambda_0/\Lambda)$ for $T = T_c = 0.13E_F$.

function of the logarithmic flow parameter $l = \ln(\Lambda_0/\Lambda)$. Our numerical result for w_Λ is for small Λ (corresponding to large l of the form $w_\lambda \propto \log(\Lambda_0/\Lambda)$). The logarithmic growth of the vertex correction at T_c can be understood analytically from the flow equation (E6), which implies that $\tilde{w}_l \propto e^{-\eta_* l}$ for large l , where η_* is the fixed point value of the anomalous dimension. In the limit of large l the flow equation (E6) therefore reduces to

$$\partial_l \tilde{w}_l \approx -\eta_* \tilde{w}_l + \text{const } e^{-\eta_* l}. \quad (\text{E18})$$

The analytic solution to this inhomogeneous differential equation is given by $\tilde{w}_l \propto l e^{-\eta_* l}$. If we scale back to the physical coupling we find $w_l \propto l$ for large l . The logarithmic divergence of a vertex correction associated with a marginal coupling at the critical point should not be surprising. Our FRG approach automatically takes care of this divergence and its feedback to the other scale-dependent couplings in the problem. The non-analytic form of the quasiparticle damping is not modified by this divergence.

- ¹ A. Larkin and A. Varlamov, *Theory of Fluctuations in Superconductors*, (Oxford University Press, Oxford, 2005).
- ² V. L. Ginzburg, *Fiz. Tverd. Tela* **2**, 2031 (1960) [*Sov. Phys. Solid State* **2**, 1824 (1961)].
- ³ A. P. Levanyuk, *Zh. Eksp. Teor. Fiz.* **36**, 810 (1959) [*Sov. Phys. JETP* **36**, 571 (1959)].
- ⁴ I. Bloch, J. Dalibard, and W. Zwerger, *Rev. Mod. Phys.* **80**, 885 (2008).
- ⁵ L. G. Aslamazov and A. I. Larkin, *Phys. Letters* **26A**, 238 (1968); L. G. Aslamazov and A. I. Larkin, *Fiz. Tverd. Tela* **10**, 1104 (1968) [*Sov. Phys. Solid State* **10**, 875 (1968)].
- ⁶ C. Di Castro, R. Raimondi, C. Castellani, and A. A. Varlamov, *Phys. Rev. B* **42**, 10211 (1990).
- ⁷ F. Palestini, A. Perali, P. Pieri, and G. C. Strinati, *Phys. Rev. B* **85**, 024517 (2012).
- ⁸ M. D. Reichl and E. J. Mueller, *Phys. Rev. A* **91**, 043627 (2015).
- ⁹ N. Lerch, L. Bartosch, and P. Kopietz, *Phys. Rev. Lett.* **100**, 050403 (2008).
- ¹⁰ L. P. Gorkov and T. K. Melik-Barkhudarov, *Zh. Eksp. Teor. Fiz.* **40**, 1452 (1961) [*Sov. Phys. JETP* **13**, 1018 (1961)].
- ¹¹ H. Heiselberg, C. J. Pethick, H. Smith, and L. Viverit, *Phys. Rev. Lett.* **85**, 2418 (2000).
- ¹² Q. Chen, J. Stajic, S. Tan, and K. Levin, *Phys. Rep.* **412**, 1 (2005).
- ¹³ S. Floerchinger, M. Scherer, S. Diehl, and C. Wetterich, *Phys. Rev. B* **78**, 174528 (2008).
- ¹⁴ Z.-Q. Yu, K. Huang, and L. Yin, *Phys. Rev. A* **79**, 053636 (2009).
- ¹⁵ A. V. Chubukov, I. Eremin, and D. V. Efremov, *Phys. Rev. B* **93**, 174516 (2016).
- ¹⁶ S. Lederer, Y. Schattner, E. Berg, and S. A. Kivelson, *Phys. Rev. Lett.* **114**, 097001 (2015).
- ¹⁷ P. Kopietz, L. Bartosch, and F. Schütz, *Introduction to the Functional Renormalization Group* (Springer, Berlin, 2010).
- ¹⁸ W. Metzner, M. Salmhofer, C. Honerkamp, V. Meden, and K. Schönhammer, *Rev. Mod. Phys.* **84**, 299 (2012).
- ¹⁹ L. Bartosch, P. Kopietz, and A. Ferraz, *Phys. Rev. B* **80**, 104514 (2009).
- ²⁰ Y. Tanizaki, G. Fejós, and T. Hatsuda, *Prog. Theor. Phys.* **2014**, 043101 (2014).
- ²¹ J. Stajic, J. N. Milstein, Q. Chen, M. L. Chiofalo, M. J. Holland, and K. Levin, *Phys. Rev. A* **69**, 063610 (2004).
- ²² C.-C. Chun, Hao Guo, Yan He, and K. Levin, *Phys. Rev. A* **81**, 023622 (2010).
- ²³ Hui Hu, Xia-Ji Liu, P. D. Drummond, and Hui Dong, *Phys. Rev. Lett.* **104**, 240407 (2010).
- ²⁴ P. Magierski, G. Wlazłowski, and A. Bulgac, *Phys. Rev. Lett.* **107**, 145304 (2011).
- ²⁵ E. J. Mueller, arXiv:1701.04838v1.
- ²⁶ J. Zinn-Justin, *Quantum Field Theory and Critical Phenomena*, (Clarendon Press, Oxford, 4th ed., 2002).
- ²⁷ C. Wetterich, *Phys. Lett. B* **301**, 90 (1993).
- ²⁸ F. Schütz, L. Bartosch, and P. Kopietz, *Phys. Rev. B* **72**, 035107 (2005).
- ²⁹ F. Schütz and P. Kopietz, *J. Phys. A: Math. Gen.* **39**, 8205 (2006).
- ³⁰ C. Drukier, L. Bartosch, A. Isidori, and P. Kopietz, *Phys. Rev. B* **85**, 245120 (2012).
- ³¹ A. Sharma and P. Kopietz, *Phys. Rev. B* **93**, 235425 (2016).
- ³² H. Gies and C. Wetterich, *Phys. Rev. D* **65**, 065001 (2002).
- ³³ E. A. Yuzbashyan, O. Tsypliyatyev, and B. L. Altshuler, *Phys. Rev. Lett.* **96**, 097005 (2006), *ibid.* **96**, 179905 (2006).
- ³⁴ E. A. Yuzbashyan and O. Tsypliyatyev, *Phys. Rev. B* **79**, 132504 (2009).
- ³⁵ C. Sträter, O. Tsypliyatyev, and A. Faribault, *Phys. Rev. B* **86**, 195101 (2012).
- ³⁶ J. P. Gaebler, J. T. Stewart, T. E. Drake, D. S. Jin, A. Perali, P. Pieri, and G. C. Strinati, *Nature Phys.* **6**, 569 (2010).

- ³⁷ K. Maki, *Prog. Theor. Phys.* **40**, 193 (1968).
- ³⁸ R. S. Thompson, *Phys. Rev. B* **1**, 327 (1970); *ibid.* **2**, 1433 (1970).
- ³⁹ J. Keller and V. Korenman, *Phys. Rev. Lett.* **27**, 1270 (1971).
- ⁴⁰ B. R. Patton, *Phys. Rev. Lett.* **27**, 1273 (1971).
- ⁴¹ A. I. Larkin and Yu. N. Ovchinnikov, *J. Low Temp. Phys.* **10**, 407 (1973).
- ⁴² C. Kittel, *Introduction to Solid State Physics* (Wiley, New York, 1996).
- ⁴³ D. J. Thouless, *Phys. Rev. Lett.* **39**, 1167 (1977).
- ⁴⁴ A. V. Chubukov, D. L. Maslov, and A. J. Millis, *Phys. Rev. B* **73**, 045128 (2006).
- ⁴⁵ S. Pelissetto and E. Vicari, *Phys. Rep.* **368**, 549 (2002).
- ⁴⁶ S. Ledowski, N. Hasselmann, and P. Kopietz, *Phys. Rev. A* **69**, 061601(R) (2004).
- ⁴⁷ N. Hasselmann, S. Ledowski, and P. Kopietz, *Phys. Rev. A* **70**, 063621 (2004).
- ⁴⁸ J. Berges, N. Tetradis, and C. Wetterich, *Phys. Rep.* **363**, 223 (2002).
- ⁴⁹ B. L. Altshuler, A. G. Aronov, and D. E. Khmel'nitsky, *J. Phys. C: Solid State Phys.* **15**, 7367 (1982).
- ⁵⁰ B. L. Altshuler, *Pis'ma Zh. Eksp. Teor. Fiz.* **41**, 530 (1985) [*JETP Letters* **41**, 648 (1985)].
- ⁵¹ B. L. Altshuler and D. E. Khmel'nitskii, *Pis'ma Zh. Eksp. Teor. Fiz.* **42**, 291 (1985) [*JETP Letters* **42**, 359 (1985)].
- ⁵² B.L. Altshuler, M. E. Gershenson, and I. L. Aleiner, *Physica E* **3**, 58 (1998).
- ⁵³ I. L. Aleiner, B. L. Altshuler, and M. E. Gershenson, *Waves in Random Media* **9**, 201 (1999).
- ⁵⁴ B. N. Narozhny, G. Zala, and I. L. Aleiner, *Phys. Rev. B* **65**, 180202(R) (2002).
- ⁵⁵ O. Tsypliyatyev, I. L. Aleiner, V. I. Falko, and I. V. Lerner, *Phys. Rev. B* **68**, 121301(R) (2003).
- ⁵⁶ V. Fal'ko, I. Lerner, O. Tsypliyatyev, and I. L. Aleiner, *Phys. Rev. Lett.* **93**, 159701 (2004).
- ⁵⁷ P. W. Anderson, *J. Phys. Chem. Solids* **11**, 26 (1959).
- ⁵⁸ A. A. Abrikosov and L. P. Gorkov, *Zh. Eksp. Teor. Fiz.* **35**, 1558 (1959) [*Sov. Phys. JETP* **8**, 1090 (1959)]; *ibid.* **36**, 319 (1959) [**9**, 220 (1959)].
- ⁵⁹ E. Dagotto, *Rev. Mod. Phys.* **66**, 763 (1994).
- ⁶⁰ D. N. Basov and T. Timusk, *Rev. Mod. Phys.* **77**, 721 (2005).
- ⁶¹ T. P. Devereaux and R. Hackl, *Rev. Mod. Phys.* **79**, 175 (2007).
- ⁶² Ø. Fischer, M. Kugler, I. Maggio-Aprile, C. Berthod, and C. Renner, *Rev. Mod. Phys.* **79**, 353 (2007).
- ⁶³ H. Alloul, J. Bobroff, M. Gabay, and P. J. Hirschfeld, *Rev. Mod. Phys.* **81**, 45 (2009).
- ⁶⁴ N. P. Armitage, P. Fournier, and R. L. Greene, *Rev. Mod. Phys.* **82**, 2421 (2010).
- ⁶⁵ A. A. Abrikosov, L. P. Gorkov, and I. Ye. Dzyaloshinskii, *Methods of Quantum Field Theory in Statistical Physics*, (Dover, New York, 1963).